nature cell biology

ARTICLES

https://doi.org/10.1038/s41556-018-0045-z

Recognition of RNA N^6-methyladenosine by IGF2BP proteins enhances mRNA stability and translation

Huilin Huang[1,2,12], Hengyou Weng[1,2,12], Wenju Sun[3,4,12], Xi Qin[1,2,12], Hailing Shi[5,6,12], Huizhe Wu[1,2,7], Boxuan Simen Zhao[5,6], Ana Mesquita[1], Chang Liu[5,6], Celvie L. Yuan[8], Yueh-Chiang Hu[8], Stefan Hüttelmaier[9], Jennifer R. Skibbe[1], Rui Su[1,2], Xiaolan Deng[1,2,7], Lei Dong[1,2], Miao Sun[10], Chenying Li[1,2,11], Sigrid Nachtergaele[5,6], Yungui Wang[1,11], Chao Hu[1,11], Kyle Ferchen[1], Kenneth D. Greis[1], Xi Jiang[1,2], Minjie Wei[7], Lianghu Qu[3,4], Jun-Lin Guan[1], Chuan He[5,6]*, Jianhua Yang[3,4]* and Jianjun Chen[1,2]*

N^6-methyladenosine (m^6A) is the most prevalent modification in eukaryotic messenger RNAs (mRNAs) and is interpreted by its readers, such as YTH domain-containing proteins, to regulate mRNA fate. Here, we report the insulin-like growth factor 2 mRNA-binding proteins (IGF2BPs; including IGF2BP1/2/3) as a distinct family of m^6A readers that target thousands of mRNA transcripts through recognizing the consensus GG(m^6A)C sequence. In contrast to the mRNA-decay-promoting function of YTH domain-containing family protein 2, IGF2BPs promote the stability and storage of their target mRNAs (for example, *MYC*) in an m^6A-dependent manner under normal and stress conditions and therefore affect gene expression output. Moreover, the K homology domains of IGF2BPs are required for their recognition of m^6A and are critical for their oncogenic functions. Thus, our work reveals a different facet of the m^6A-reading process that promotes mRNA stability and translation, and highlights the functional importance of IGF2BPs as m^6A readers in post-transcriptional gene regulation and cancer biology.

As the most abundant messenger RNA (mRNA) modification, N^6-methyladenosine (m^6A) modification is reversible and plays critical roles in multiple fundamental biological processes (for example, cell differentiation, tissue development and tumorigenesis)[1–13]. High-throughput sequencing revealed that m^6A is especially enriched in the 3′ untranslated regions (UTRs) and near the stop codons of mRNAs with a consensus sequence of RRACH (R corresponds to G or A; H corresponds to A, C or U)[2,3]. The biological importance of m^6A modification relies on m^6A-binding proteins (that is, readers). Thus, it is crucial to identify and characterize m^6A readers that directly guide distinct bioprocesses. A group of YT521-B homology (YTH) domain-containing proteins (YTHDFs) have been identified as m^6A readers that control mRNA fate by regulating pre-mRNA splicing, facilitating translation or promoting mRNA decay[2,10,14–16].

In the YTHDF2-mediated decay pathway[10], mRNA levels are expected to increase when m^6A abundance is reduced. However, our recent data showed that a large portion of mRNAs with reduced m^6A abundance tended to be downregulated due to decreased RNA stability[12], suggesting the presence of alternative mechanisms to stabilize m^6A-modified mRNAs. Here, we report the insulin-like growth factor 2 (IGF2) mRNA-binding proteins 1, 2 and 3 (IGF2BP1/2/3) as a new family of m^6A readers that guard m^6A-modified mRNAs from decay. IGF2BPs, a conserved family of single-stranded RNA-binding proteins (RBPs)[17], are composed of six canonical RNA-binding domains, including two RNA recognition motif (RRM) domains and four K homology (KH) domains[17,18]. Besides *IGF2*, a few other well-known mRNAs (for example, *MYC*, *ACTIN* and *LIN28B*) have been reported as targets of IGF2BPs[19–21]. However, the exact molecular mechanisms by which IGF2BPs recognize and regulate the expression of their targets remain elusive. Here, we provide compelling evidence showing that IGF2BPs preferentially recognize m^6A-modified mRNAs and promote the stability (and probably also translation) of thousands of potential mRNA targets (including *MYC*) in an m^6A-dependent manner, thereby globally affecting gene expression output. Furthermore, as m^6A readers, IGF2BPs play oncogenic roles in cancer cells, probably by stabilizing methylated mRNAs of oncogenic targets (for example, *MYC*).

Results

Identification of IGF2BPs as m^6A-binding proteins. To identify m^6A-binding proteins, we applied two independent methods:

[1]Department of Cancer Biology, University of Cincinnati College of Medicine, Cincinnati, OH, USA. [2]Department of Systems Biology, City of Hope, Monrovia, CA, USA. [3]Key Laboratory of Gene Engineering of the Ministry of Education, Sun Yat-sen University, Guangzhou, China. [4]State Key Laboratory for Biocontrol, Sun Yat-sen University, Guangzhou, China. [5]Department of Chemistry and Institute for Biophysical Dynamics, The University of Chicago, Chicago, IL, USA. [6]Howard Hughes Medical Institute, The University of Chicago, Chicago, IL, USA. [7]Department of Pharmacology, School of Pharmacy, China Medical University, Shenyang, China. [8]Division of Developmental Biology, Cincinnati Children's Hospital Medical Center, Cincinnati, OH, USA. [9]Institute of Molecular Medicine, Department of Molecular Cell Biology, Martin Luther University, Halle, Germany. [10]Division of Human Genetics, Cincinnati Children's Hospital Medical Center, Cincinnati, OH, USA. [11]Key Laboratory of Hematopoietic Malignancies, Department of Hematology, The First Affiliated Hospital of Zhejiang University, Hangzhou, China. [12]These authors contributed equally: Huilin Huang, Hengyou Weng, Wenju Sun, Xi Qin and Hailing Shi. *e-mail: chuanhe@uchicago.edu; yangjh7@mail.sysu.edu.cn; jianchen@coh.org

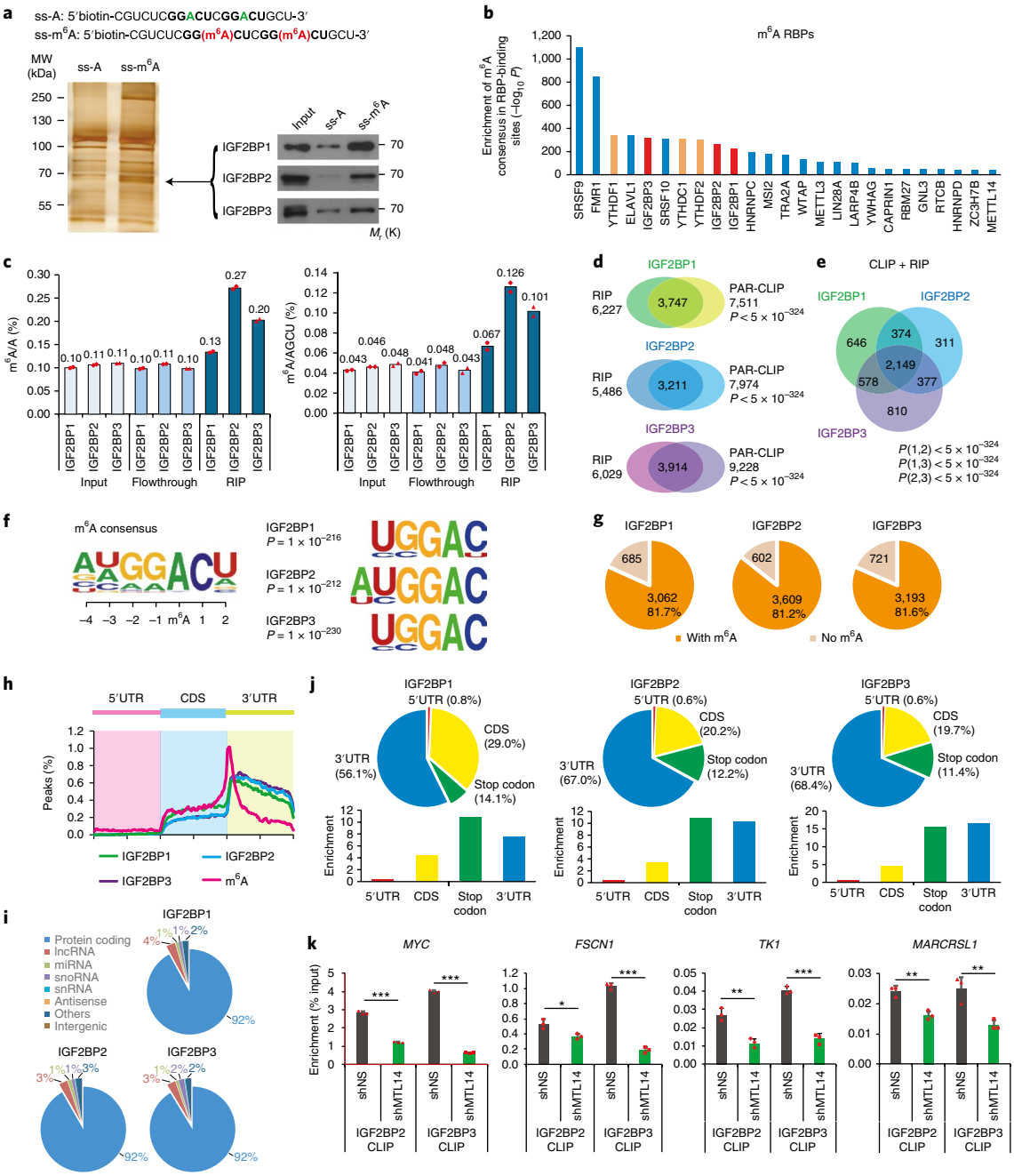

Fig. 1 | Selective binding of IGF2BPs to m⁶A-modified RNAs. a, Identification of m⁶A-specific binding proteins by RNA affinity chromatography using single-stranded RNA probes with methylated (red) or unmethylated (green) adenosine. Consensus sequence shown in bold. Silver staining (left) and western blotting (right) showed selective pulldown of ~68 kDa IGF2BP proteins from the HEK293T nuclear extract. Western blot images are representative of three independent experiments. **b**, Enrichment of the m⁶A consensus sequence 'GGAC' in the binding sites of RBPs. The three IGF2BP paralogues are shown in red, whereas the YTHDFs were shown in orange. *P* values were calculated based on the binomial test by the Homer software. **c**, Quantification of m⁶A/A and m⁶A/AGCU ratios by LC-MS/MS in RNAs bound by ectopically expressed IGF2BP1 (chicken ZBP1), IGF2BP2 (human) or IGF2BP3 (human). Values are the mean of $n = 2$ independent experiments, and individual data points are showed. **d**, Overlap of IGF2BP target genes identified by RIP-seq and published PAR-CLIP in HEK293T cells. RIP-seq was performed once. *P* values were calculated by Fisher's test. **e**, Venn diagram showing the numbers of shared high-confidence targets (that is, CLIP + RIP targets) among IGF2BP paralogues. *P* values were calculated by Fisher's test. **f**, Top consensus sequences of IGF2BP-binding sites and the m⁶A motif detected by HOMER motif analysis with PAR-CLIP data. **g**, Pie charts showing the numbers and percentages of IGF2BP high-confidence target genes that contain m⁶A peaks. The m⁶A-seq data were reported in ref.[3]. **h**, Metagene profiles of enrichment of IGF2BP-binding sites and m⁶A modifications across mRNA transcriptome. CDS, coding sequence. **i**, Percentages of various RNA species bound by IGF2BPs. lncRNA, long non-coding RNA; miRNA, microRNA; snRNA, small nuclear RNA; snoRNA, small nucleolar RNA. **j**, The distribution (top) and enrichment (bottom) of IGF2BP-binding peaks within different gene regions. Enrichment was determined by the proportion of IGF2BP-binding peaks normalized by the length of the region. Analyses in panels **i** and **j** were performed twice with similar results. **k**, In vivo binding of FLAG–IGF2BP2 to representative target genes in *METTL14*-knockdown or control HEK293T cells. Values are the mean ± s.d. of $n = 3$ independent experiments. $^{*}P < 0.05$; $^{**}P < 0.01$; $^{***}P < 0.001$; two-tailed Student's *t*-test. Unprocessed scans of western blot analysis are available in Supplementary Fig. 8. Source data for **c** and **k** are in Supplementary Table 3.

(1) using methylated single-stranded RNA bait (ss-m^{6}A, with the consensus sequence GG(m^{6}A)CU) or unmethylated control RNA (ss-A) for RNA pull-down (Fig. 1a and Supplementary Fig. 1a), followed by mass spectrometry analysis[2]; and (2) developing a computational pipeline for screening potential m^{6}A-binding proteins by using published RBP crosslinking and immunoprecipitation followed by high-throughput sequencing (CLIP–seq) data sets and known m^{6}A modification sites[3]. All three IGF2BP proteins were identified by mass spectrum and were confirmed to selectively bind to the methylated bait (ss-m^{6}A) with a 3–4-fold higher affinity than the unmethylated control (ss-A) (Fig. 1a and Supplementary Fig. 1b), and the binding seems to be independent of RNA secondary structure (Supplementary Fig. 1c). Similar to endogenous proteins, recombinant IGF2BP proteins purified from human cells also preferentially bound to methylated RNA probe over the unmethylated one (Supplementary Fig. 1d,e). In addition to ss-m^{6}A, IGF2BPs also preferentially bound to methylated hairpin RNA (hp-m^{6}A) probes over control (hp-A) probes (Supplementary Fig. 1f,g). Meanwhile, our computational pipeline revealed that all three IGF2BPs were among the top 15 of 112 RBPs in terms of both the significance (Fig. 1b) and the frequency (Supplementary Fig. 1h) of m^{6}A motifs enriched in their RNA-binding sites. Thus, IGF2BP proteins are potential m^{6}A-binding proteins.

We then overexpressed FLAG-tagged IGF2BPs in HEK293T cells and immunoprecipitated ribonucleoprotein complexes to evaluate the in cellulo binding. A significant enrichment of m^{6}A modifications in FLAG-IGF2BPs-bound RNA was observed (Fig. 1c and Supplementary Fig. 1i), similar to that in RNA immunoprecipitates (RIPs) of endogenous IGF2BPs (Supplementary Fig. 1j). Sequencing purified RNA from FLAG-RIP samples identified >5,000 genes from each RIP sample; among them, >50% overlapped with published photoactivatable ribonucleoside-enhanced (PAR)-CLIP–seq targets[22] ($P < 5 \times 10^{-324}$, Fisher's exact test; Fig. 1d). The 3,747, 3,211 and 3,914 transcripts identified by both RIP and PAR-CLIP methods can be considered as high-confidence targets of IGF2BP1, IGF2BP2 and IGF2BP3, respectively (Fig. 1d and Supplementary Table 1). The three IGF2BP proteins shared 2,149 (55–70%) high-confidence RNA targets (Fig. 1e). All three IGF2BPs preferentially bind to the 'UGGAC' consensus sequence containing the 'GGAC' m^{6}A core motif (Fig. 1f), and >80% of the high-confidence targets contain at least one m^{6}A peak as detected by m^{6}A-seq[3] (Fig. 1g). Moreover, most of the IGF2BP-binding sites (92%) are located in protein-coding transcripts (that is, mRNAs) and are highly enriched near stop codons and in 3′UTRs, coinciding with the m^{6}A distribution (Fig. 1h–j). In addition, we analysed ENCODE (Encyclopedia of DNA Elements) enhanced CLIP (eCLIP)–seq data in HepG2 cells and human embryonic stem cells (hESCs), and found that the 'UGGAC' motif was also enriched in the targets of IGF2BPs in both cell types (Supplementary Fig. 1k.l).

Methyltransferase-like protein 3 (METTL3) and METTL14 are two critical components of the methyltransferase complex, which catalyses methylation at N^6-adenosine. We performed CLIP of FLAG-tagged IGF2BP2 and IGF2BP3 in HEK293T cells with or without *METTL14* knockdown. Four representative high-confidence targets, including *MYC*, *FSCN1*, *TK1* and *MARCKSL1*, exhibit strong binding with IGF2BPs around their m^{6}A motifs in control cells (Fig. 1k). Such binding was largely impaired upon *METTL14* knockdown (Fig. 1k), suggesting that there is a requirement of cellular m^{6}A modification for the binding. Taken together, these data demonstrated the role of IGF2BPs as m^{6}A-binding proteins in vitro and in cellulo.

Silencing of IGF2BPs globally downregulates target gene expression. We next conducted RNA sequencing (RNA-seq) in individual *IGF2BP*-knockdown and control HepG2 cells (Supplementary Fig. 2a). The global transcripts were grouped into non-targets, CLIP targets and CLIP + RIP targets according to their binding by IGF2BPs in HEK293T cells (see Fig. 1d), considering the availability of CLIP data for all three IGF2BPs in this cell line. Knockdown of individual IGF2BPs globally and preferentially inhibited the expression of CLIP targets and especially of CLIP + RIP targets, with much more CLIP + RIP targets being downregulated than upregulated (Fig. 2a,b). Gene-set enrichment analysis (GSEA) also showed that genes highly expressed in the control groups were enriched with the IGF2BP CLIP + RIP targets (false discovery rate (FDR) < 0.05; Supplementary Fig. 2b). Functional annotation indicated that target genes with reduced expression were enriched in DNA replication, cell cycle, proliferation and cancer-related biological processes and pathways (Supplementary Fig. 2c). In addition, an enrichment of cell cycle genes and MYC target genes was observed in controls versus short hairpin IGF2BPs (shIGF2BPs; Supplementary Fig. 2d). Downregulation of representative targets was confirmed by quantitative PCR (qPCR; Fig. 2c).

To determine whether the expression of IGF2BP targets is also affected by the level of cellular m^{6}A, we performed m^{6}A-seq and RNA-seq in control or *METTL14*-knockdown HepG2 cells. Upon *METTL14* knockdown, 1,516 genes showed reduced m^{6}A modifications (that is, m^{6}A-Hypo genes; fold change (FC) < 0.667). Among these genes, 418 had reduced (that is, m^{6}A-Hypo-down genes; FC < 0.8) mRNA levels, whereas 335 had increased levels (that is, m^{6}A-Hypo-up genes; FC > 1.2) (Fig. 2d). As expected, IGF2BP high-confidence targets showed a global and significant reduction in mRNA level upon *METTL14* knockdown (Fig. 2e). The expression of individual targets, including *FSCN1*, *TK1*, *MARCKSL1* and *MYC*, was confirmed by qPCR to be significantly downregulated upon *METTL3* or *METTL14* knockdown (Fig. 2f). Similar changes were observed for *FSCN1* and *MYC*, two shared targets of IGF2BPs and YTHDF2, in *IGF2BP1/YTHDF2* double-knockdown cells (Supplementary Fig. 2e). Conversely, the m^{6}A-Hypo-down genes were globally downregulated upon knockdown of *IGF2BPs*, as compared to their non-target counterparts (Supplementary Fig. 2f). The correlated regulation of gene expression by IGF2BPs and METTL14 indicates that IGF2BPs are responsible for the expression output of m^{6}A-regulated genes.

Regulation of mRNA stability by IGF2BPs. mRNA stability profiling in HepG2 cells revealed that high-confidence targets of IGF2BP1–3 tend to have longer half-lives ($P < 0.001$) than their non-target counterparts (Fig. 3a), whereasYTHDF2 targets tend to have shorter half-lives (Supplementary Fig. 3a). Similar results were observed in HeLa cells[10] (Fig. 3a and Supplementary Fig. 3a). As IGF2BP3 silencing affected target gene expression most potently (Fig. 2a,b), we performed mRNA stability profiling in *IGF2BP3*-knockdown cells. The median half-life of IGF2BP3 high-confidence targets as well as CLIP targets was significantly reduced in IGF2BP3-depleted cells to approximately 50% of that in control cells (Fig. 3b,c and Supplementary Fig. 3b,c). Accelerated mRNA decay of *MYC*, *FSCN1*, *TK1* and *MARCKSL1* upon knockdown of each *IGF2BP* was confirmed in HepG2 cells (Fig. 3d and Supplementary Fig. 3d) and human cord blood CD34$^+$ cells (Supplementary Fig. 3e). Furthermore, the stability of *MYC*, *FSCN1*, *TK1* and *MARCKSL1* mRNAs was also reduced when m^{6}A writers were silenced (Fig. 3e and Supplementary Fig. 3f).

To identify co-factors of IGF2BPs that may enhance stability of mRNA targets, we pulled down the IGF2BP2 complexes and conducted mass spectrometry analysis. Notably, ELAV-like RNA-binding protein 1 (ELAVL1; also known as HuR), matrin 3 (MATR3) and poly(A)-binding protein cytoplasmic 1 (PABPC1), three known mRNA stabilizers[23–26], were identified. Western blotting confirmed their binding to ectopically expressed IGF2BPs in HEK293T cells (Fig. 3f), consistent with previous reports[21,27]. Moreover, co-localization of HuR and IGF2BPs was observed in cytoplasmic granules

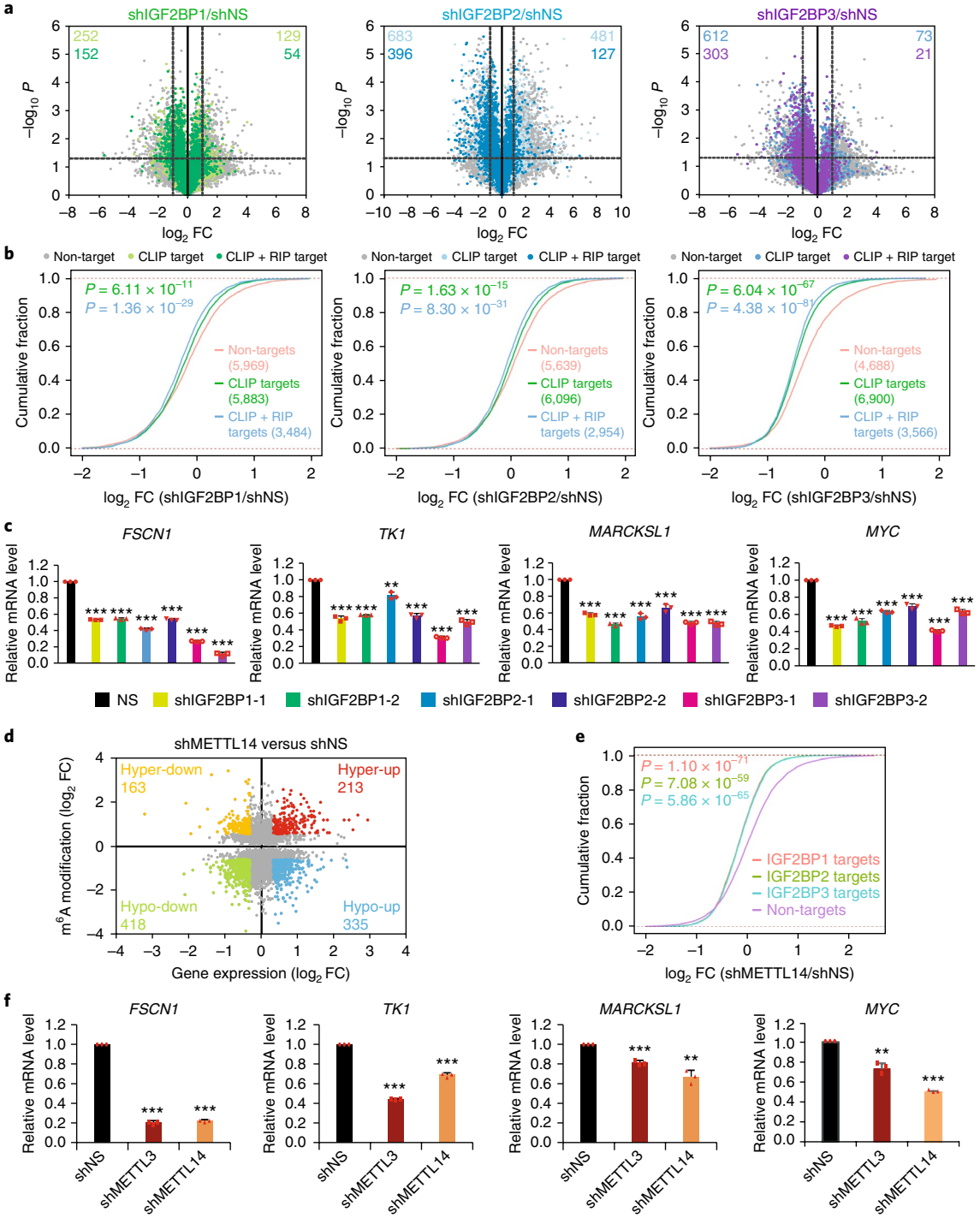

Fig. 2 | IGF2BPs regulate transcriptome-wide mRNA levels. a, Volcano plots displaying enrichment of dysregulated target genes in *IGF2BP*-knockdown (shIGF2BP) versus control (shNS) HepG2 cells. The numbers of significantly downregulated ($\log_2$ FC < −1, $P < 0.05$, two-tailed Student's *t*-test) or upregulated ($\log_2$ FC > 1, $P < 0.05$, two-tailed Student's t-test) genes in the CLIP target group and CLIP + RIP target group are shown. Vertical dashed lines indicate cutt-off of $\log_2$FC (1 or -1), whereas the horizontal dashed lines indicate cut-off of *P* value (0.05). FC, fold change **b**, Cumulative frequency of mRNA $\log_2$ FC in non-target, CLIP target and CLIP + RIP target genes upon *IGF2BP* silencing. *P* values were calculated using two-sided Wilcoxon and Mann–Whitney test. **c**, Relative changes in *FSCN1*, *TK1*, *MARCKSL1* and *MYC* mRNA levels upon *IGF2BP* silencing. Results from two shRNAs for each *IGF2BP* are shown. Values are the mean ± s.d. of $n = 3$ independent experiments. Two-tailed Student's *t*-tests were used (**$P < 0.01$; ***$P < 0.001$). **d**, Distribution of genes with a significant change in both the m^{6}A level and the gene expression level in *METTL14*-knockdown HepG2 cells compared with control cells. **e**, Cumulative frequency of mRNA $\log_2$ FC showing global reduction of IGF2BP high-confidence target genes in shMETTL14 versus shNS cells. *P* values were calculated using two-sided Wilcoxon and Mann–Whitney test. Exponential regression was used in panels **d** and **e**. Gene expression in panels **a** and **b** were analysed three times, whereas panel **e** was analysed twice. **f**, Relative changes in *FSCN1*, *TK1*, *MARCKSL1* and *MYC* mRNA levels upon *METTL3* or *METL14* silencing. Values are the mean ± s.d. of $n = 3$ independent experiments. Two-tailed Student's *t*-tests were used (**$P < 0.01$; ***$P < 0.001$). Source data for **c** and **f** are in Supplementary Table 3.

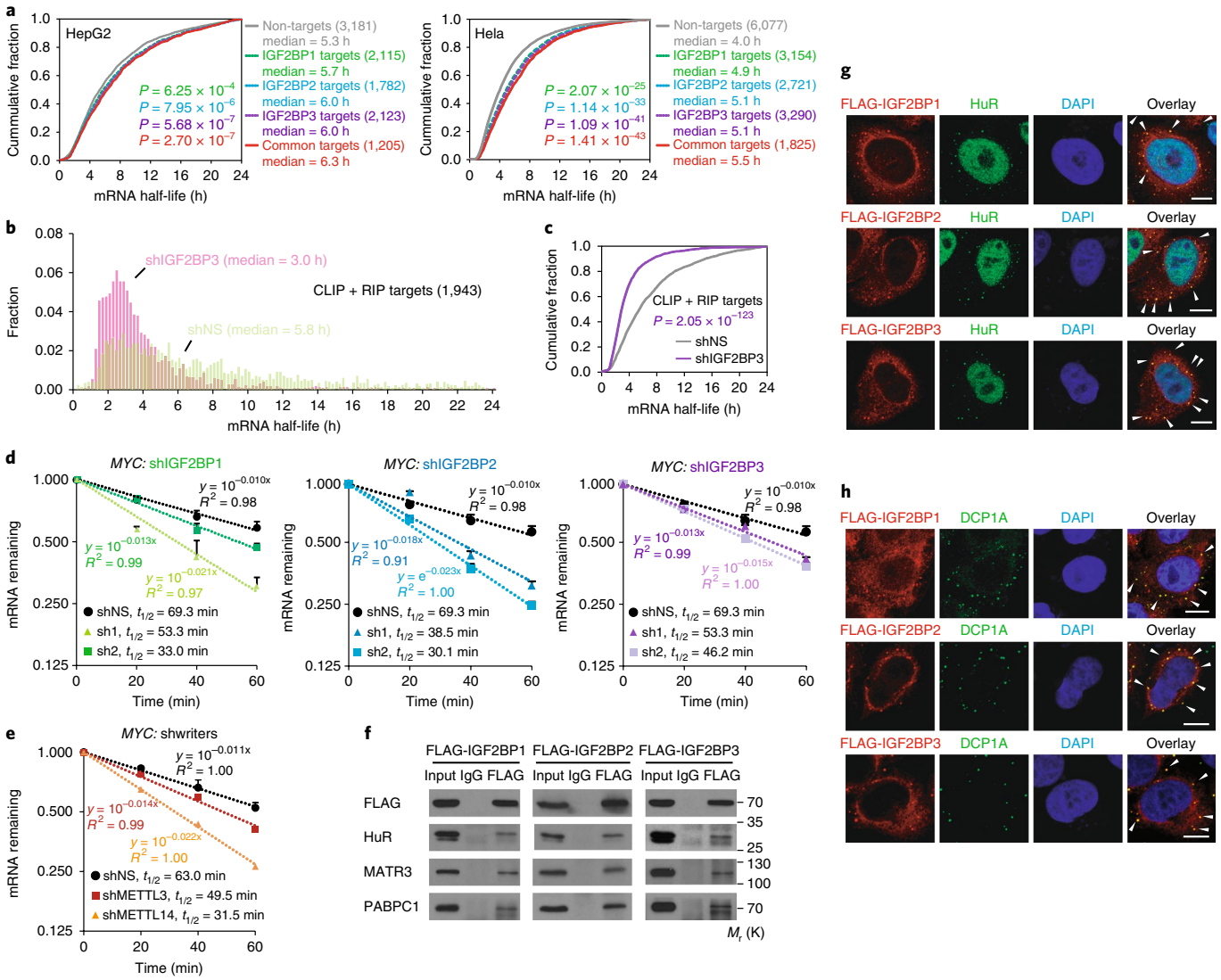

Fig. 3 | Knockdown of IGF2BPs decreases mRNA stability. a, Cumulative distribution of mRNA half-lives of non-target or IGF2BP high-confidence target genes in HepG2 and HeLa cells. **b**, Distribution of mRNA half-lives in IGF2BP3 high-confidence targets in HepG2 cells with shIGF2BP3 or shNS. **c**, Cumulative distribution of mRNA half-life of IGF2BP3 high-confidence targets in shIGF2BP3 or shNS HepG2 cells. mRNA half-life analyses in panels **a**–**c** were repeated twice. **d**,**e**, Reducing *MYC* mRNA half-life by silencing *IGF2BPs* (**d**) or m^{6}A writers (**e**) in HepG2 cells. Values are the mean ± s.d. of $n = 3$ independent experiments. **f**, Co-immunoprecipitation and western blotting showing the binding of mRNA stabilizers with FLAG-tagged IGF2BPs in HEK293T cells, representative of three independent experiments. **g**,**h**, Co-localization of IGF2BP proteins with HuR (**g**) or DCP1A (**h**) in HeLa cells. Arrowheads indicate co-localization in cytoplasmic granules. Scale bars, 10 μm. Images are representative of three independent experiments. *P* values were calculated using two-sided Wilcoxon and Mann–Whitney test in panels **a**–**c**. Unprocessed scans of western blot analysis are available in Supplementary Fig. 8. Source data for **d** and **e** are in Supplementary Table 3.

(Fig. 3g), which was highly likely in processing bodies (P-bodies), as shown by DCP1A (a P-body marker) staining (Fig. 3h). Thus, IGF2BPs probably recruit RNA stabilizers to promote the stability of their mRNA targets.

Stress granules are a second type of cytoplasmic messenger ribonucleoprotein granule thought to protect mRNAs from harmful conditions, and the protected mRNAs could be returned for translation after stress is relieved. We found that IGF2BPs were well co-localized with the stress granule marker TIAR, but only partially overlapped with DCP1A under heat shock (Supplementary Fig. 3g,h), which is consistent with previous reports[28,29] and further reveals the roles of IGF2BPs in mRNA stabilization and storage during stress. Thus, our data indicate that IGF2BPs can promote RNA stability and/or increase mRNA storage in a dynamic manner under different physiological conditions.

Polysome profiling showed that FLAG-IGF2BP1 and FLAG-IGF2BP2 were present in most of the sucrose gradient fractions, whereas FLAG-IGF2BP3 was accumulated in 60S and 40S (Supplementary Fig. 4a). A similar distribution of endogenous IGF2BP1/2/3 proteins was observed in HepG2 cells (Supplementary Fig. 4b). Interestingly, HuR was detected along with each FLAG-tagged IGF2BP (Supplementary Fig. 4a). Moreover, knockdown of *IGF2BP1* in HEK293T cells significantly reduced *MYC* mRNA in the translating pool (Supplementary Fig. 4c, fractions 13–18), suggesting a role of IGF2BPs in the active translation of their target genes. In agreement with the localization of IGF2BPs to stress granules during heat shock, IGF2BP2 shifted to non-ribosome fractions, and was found to gradually return to ribosome fractions during recovery from heat shock (Supplementary Fig. 4d).

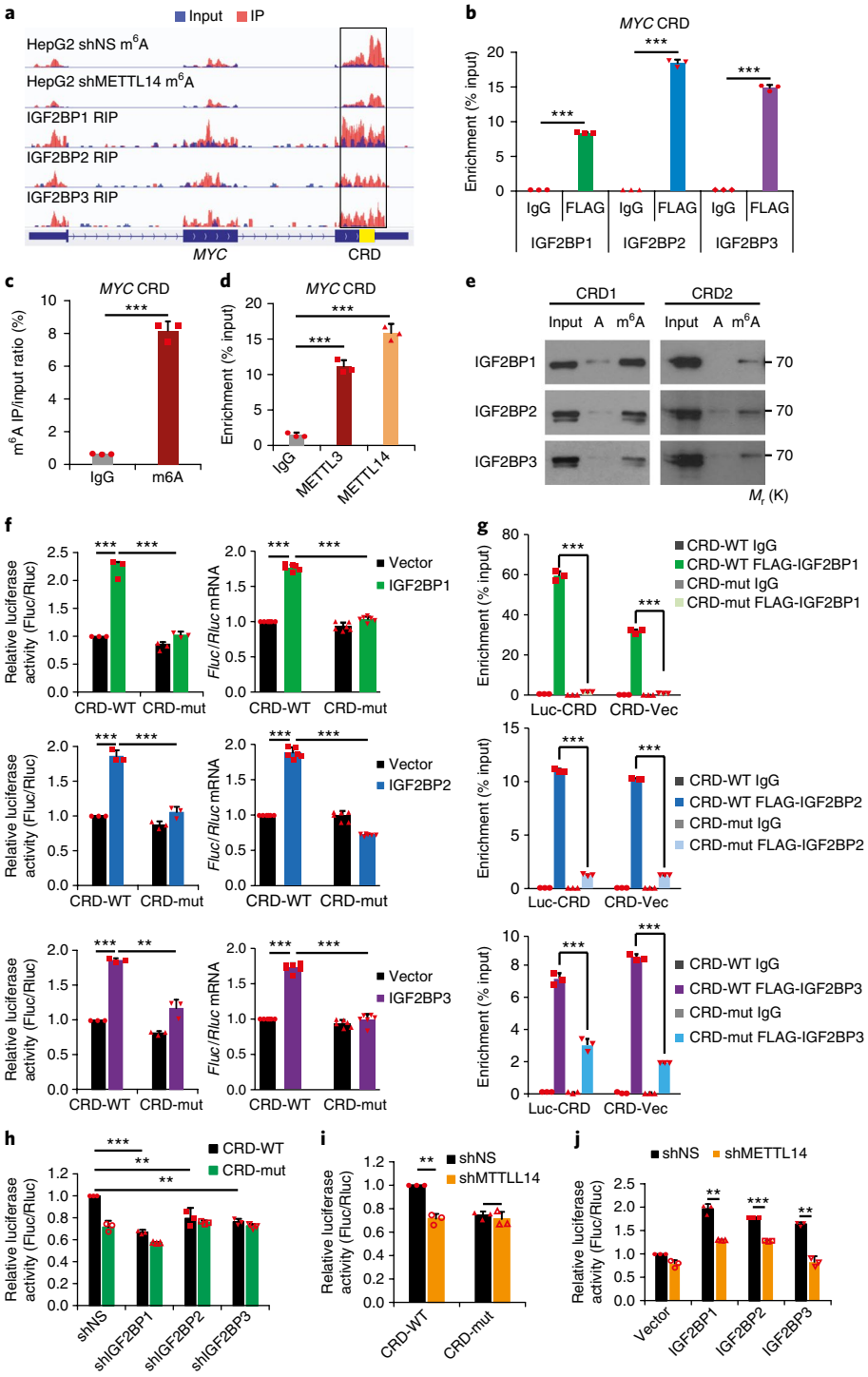

Fig. 4 | IGF2BPs regulate *MYC* expression through binding to methylated CRD. a, Distribution of m^{6}A peaks across *MYC* mRNA transcript. The CRD region is highlighted in yellow. m^{6}A-seq was repeated twice, whereas RIP–seq was performed once. IP, immunoprecipitation. **b**, RIP–qPCR showing the association of *MYC* CRD with FLAG-tagged IGF2BPs in HEK293T cells. **c**, Enrichment of m^{6}A modification in *MYC* CRD as detected by a gene-specific m^{6}A qPCR assay. **d**, RIP–qPCR showing the binding of METTL3 and METTL14 to the *MYC* CRD. **e**, RNA pulldown of endogenous IGF2BP proteins from HEK293T nuclear extract using synthetic CRD RNA fragments, CRD1 and CRD2, with (m^{6}A) or without (A) m^{6}A modifications. Images are representative of three independent experiments. **f**, Relative Fluc activity (that is, protein level) and *Fluc* mRNA level of wild-type (CRD-WT) or mutated (CRD-mut) CRD reporters in HEK293T cells with ectopically expressed IGF2BP1, IGF2BP2 or IGF2BP3. **g**, RIP–qPCR detecting the in vivo binding of FLAG-IGF2BPs to the transcripts of CRD-WT or CRD-mut luciferase reporter in HEK293T cells. **h**,**i**, Relative luciferase activity of CRD-WT or CRD-mut in HeLa cells with or without stable knockdown of *IGF2BPs* (**h**) or *METTL14* (**i**). **j**, Relative luciferase activity of CRD-WT or CRD-mut in *METTL14* stable knockdown or control HeLa cells with ectopic expression of *IGF2BPs*. For all luciferase assays, the Fluc/Rluc ratio (representing luciferase activity) of CRD-WT with empty vector or shNS was used for normalization. Values are the mean ± s.d. of $n = 3$ independent experiments, and two-tailed Student's *t*-tests were used in **b**–**d** and **f**–**j**. (**$P < 0.01$; ***$P < 0.001$). Unprocessed scans of western blot analysis are available in Supplementary Fig. 8. Source data for **b**–**d** and **f**–**j** are in Supplementary Table 3.

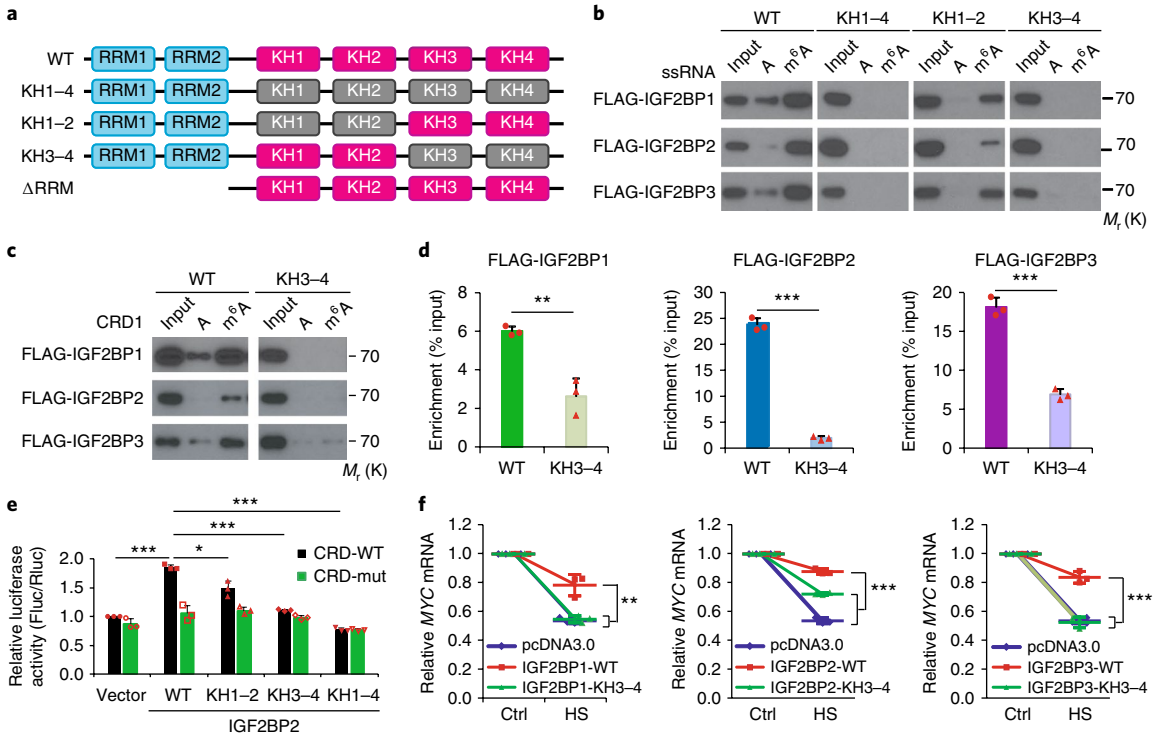

Fig. 5 | The KH domains of IGF2BPs are critical for m^{6}A recognition and binding. a, Schematic structures showing RNA-binding domains within IGF2BP proteins and a summary of IGF2BP variants used in this study. Blue boxes are RRM domains, red boxes are wild-type KH domains with GxxG core and grey boxes are inactive KH domains with GxxG to GEEG conversions. **b**, RNA pulldown followed by western blotting showed in vitro binding of single-stranded RNA (ssRNA) baits with wild-type or KH domain-mutated IGF2BP variants, representative of three independent experiments. **c**, In vitro binding of CRD1 RNA probes with wild-type or KH3–4-mutated IGF2BPs, representative of three independent experiments. **d**, The association of wild-type and KH3–4-mutated IGF2BPs with *MYC* CRD in HEK293T cells, as assessed by RIP–qPCR. **e**, Relative luciferase activity of CRD reporters in HEK293T cells with forced expression of wild-type or mutated IGF2BP2 variants. **f**, Changes in *MYC* mRNA levels in HeLa cells with empty vector or forced expression of wild-type or KH3–4-mutated IGF2BPs 1 h post-heat shock (HS). Ctrl, control. Values are the mean ± s.d. of $n = 3$ independent experiments, and two-tailed Student's *t*-tests were used in **d**–**f** (*$P < 0.05$; **$P < 0.01$; ***$P < 0.001$). Unprocessed scans of western blot analysis are available in Supplementary Fig. 8. Source data for **d**–**f** are in Supplementary Table 3.

IGF2BPs regulate *MYC* expression in an m^{6}A-dependent manner. To determine whether IGF2BP-mediated gene regulation is m^{6}A dependent, we chose *MYC*, a well-known target of IGF2BP1 (refs [19,21,30]), for a systematic study. A approximately 250 nucleotide (nt) *cis*-acting element called coding region instability determinant (CRD) resides in the 3′ terminus of the *MYC* coding region and has been proven to be critical for IGF2BP1 binding[30]. As shown in Fig. 4a, m^{6}A modifications are accumulated across *MYC* transcript, and the m^{6}A peaks coincide well with IGF2BP-binding sites. Notably, the CRD-containing region has a high abundance of m^{6}A modifications that decreases remarkably upon *METTL14* knockdown (Fig. 4a). By conducting RIP and gene-specific m^{6}A assays, we confirmed in cellulo IGF2BP binding (Fig. 4b and Supplementary Fig. 5a) and m^{6}A modification (Fig. 4c), as well as METTL3 and METTL14 binding (Fig. 4d), in CRD. Moreover, the m^{6}A modifications in the consensus sites of the synthetic CRD RNA oligos greatly facilitated their binding by endogenous IGF2BPs (Fig. 4e).

We next inserted the 249-nt wild-type or mutant CRD sequence into a firefly luciferase (Fluc) reporter (Supplementary Fig. 5b). Mutations in the m^{6}A sites of CRD (CRD1 and CRD2 RNA oligos) dramatically abrogated the association with IGF2BP proteins in vitro (Supplementary Fig. 5c). As expected, ectopic IGF2BPs induced a significant increase in Fluc activity of the wild-type reporter in a dose-dependent manner (Supplementary Fig. 5d). Such increases were largely impaired by mutations in the m^{6}A consensus sites (Fig. 4f, left, and Supplementary Fig. 5b). Consistently, the relative *Fluc* mRNA level of reporters with wild-type CRD, but not those with mutant CRD, was increased by *IGF2BP* overexpression (Fig. 4f, right). RIP-qPCR demonstrated a strong binding of IGF2BPs with wild-type CRD reporters and a much less or no binding with mutant CRD in cellulo (Fig. 4g). Conversely, knockdown of individual *IGF2BPs*, similar to knockdown of *METTL14*, caused inhibited Fluc activity, which also relies on the presence of wild-type m^{6}A motifs within CRD (Fig. 4h,i). Noticeably, IGF2BP-mediated increase of luciferase activity could be partially or completely blocked by *METTL14* knockdown (Fig. 4j). Taken together, our data demonstrate that m^{6}A modifications in CRD are required for the binding of IGF2BPs to *MYC* and for IGF2BP-mediated regulation of *MYC* expression.

Recognition of m^{6}A by the KH domains of IGF2BPs. RRM and KH, the RNA-binding domains of IGF2BPs, are different from the YTH domain, the known m^{6}A-binding domain[2,10,14,16]. We constructed IGF2BP mutants with truncation of the two RRM domains, or with mutations of GxxG to GEEG in the KH domains as reported[20] (Fig. 5a), and showed that mutations in the KH domains (KH1–4), but not RRM truncation, completely abolished the interaction between IGF2BPs and ss-m^{6}A probes (Fig. 5b and Supplementary Fig. 5e). Interaction of IGF2BPs with ss-m^{6}A probes was only partially reduced by KH1–2 di-domain mutation, but was almost completely abolished by KH3–4 mutation (Fig. 5b), indicating that the KH3–4 di-domain is indispensable for m^{6}A recognition and binding, whereas KH1–2 might play an accessory role. KH domain mutations, including KH3–4 and KH1–4, but less likely KH1–2

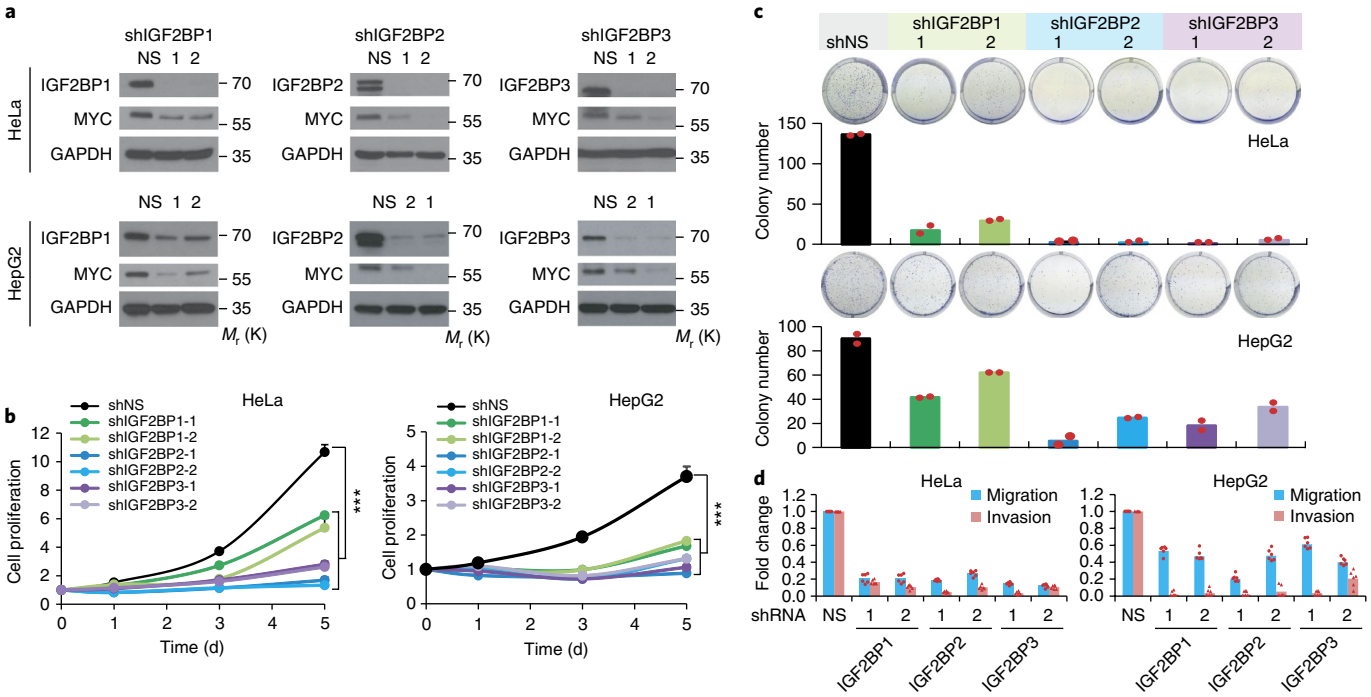

Fig. 6 | The oncogenic functions of IGF2BPs in human cancer cells. a, Western blot showing depletion of MYC protein in *IGF2BP*-silenced HeLa and HepG2 cells, representative of three independent experiments. **b**, Inhibition of cell proliferation in *IGF2BP*-silenced cells compared with control cells as determined by MTT assays. Values are the mean ± s.d. of $n = 3$ independent experiments. Two-tailed Student's *t*-tests were used (***$P < 0.001$). **c**, Effect of *IGF2BP* silencing on colony formation ability. Representative images of crystal violet staining of cells in 6-well plates are shown on top of the histograms. Colonies were counted from three replicate wells, and two independent experiments were performed. The colony number of each experiment represents the total count of three replicate wells. **d**, Repression of migration and invasion by shRNAs against *IGF2BPs*. Numbers of migrated or invaded cells were counted from three replicate wells, and two independent experiments were performed. The numbers in the control (shNS) groups were set as 1. Unprocessed scans of western blot analysis are available in Supplementary Fig. 8. Source data for **b**–**d** are in Supplementary Table 3.

mutation or RRM truncation, also impaired the binding of IGF2BP2 to hp-m^{6}A probes (Supplementary Fig. 5f). Accordingly, mutation of KH3–4 interrupted the association of IGF2BPs with methylated CRD probes in vitro and with *MYC* CRD in cellulo (Fig. 5c,d). Moreover, IGF2BP2-promoted luciferase expression of the wild-type CRD reporter was partially impaired by KH1–2 mutation and completely diminished by KH3–4 or KH1–4 mutations (Fig. 5e).

IGF2BP1 was reported to play a role in stabilizing mRNA under stress conditions[29,31]. We found that when HeLa cells were exposed to heat shock at 42 °C for 1 h and *MYC* mRNA was decreased to about 50% (Fig. 5f). Overexpression of wild-type IGF2BPs significantly diminished the reduction of *MYC* mRNA; however, this protective effect was largely or completely impaired by the mutation in KH3–4 (Fig. 5f). Collectively, these results demonstrate the essential roles of KH3–4 di-domains in IGF2BP binding to m^{6}A-modified mRNAs and in the regulation of target gene expression under both normal and stress conditions.

IGF2BPs play oncogenic roles in cancers as m^{6}A readers. Detailed analysis of public databases from the cBioPortal for Cancer Genomics (http://www.cbioportal.org) and The Cancer Genome Atlas (TCGA) (http://cancergenome.nih.gov) showed that all three IGF2BPs are frequently amplified or highly expressed in various human cancers (Supplementary Fig. 6a,b). Given their similar effect on stabilizing oncogenic transcripts such as *MYC*, we assume that all three IGF2BPs could exert oncogenic functions in cancer. Indeed, knocking down of each individual *IGF2BPs* in HeLa (cervical cancer) and HepG2 (liver cancer) cells significantly repressed MYC expression (Fig. 6a) and inhibited cancer cell proliferation, colony formation ability and cell migration/invasion (Fig. 6b–d and Supplementary Fig. 6c–e), which mimics the effect of *MYC* silencing (Supplementary Fig. 6f–j).

By utilizing the clustered regularly interspaced short palindromic repeats (CRISPR)–CRISPR-associated protein 9 (Cas9) system, we generated IGF2BP-knockout (KO) cells (Fig. 7a) and performed rescue experiments. The decreased proliferation and colony formation ability of KO cells could be reversed by forced expression of wild-type IGF2BPs, but not the KH3–4 mutants (Fig. 7b,c), suggesting that the oncogenic function of IGF2BPs relies on their role as m^{6}A readers. Ectopic expression of MYC also restored the proliferative ability of IGF2BP-KO cells (Fig. 7d), which further supports *MYC* as a critical target of IGF2BPs.

Discussion

The characterization of the YTHDFs as direct m^{6}A readers [2,10,14,16] has provided profound insights into our understanding of the effects of m^{6}A modification on genetic information flow. Our findings add a distinct RBP family, IGF2BPs, into the catalogue of m^{6}A readers, and reveal their roles in mRNA stabilization and translation (Fig. 7e). Notably, >3,000 mRNA transcripts were identified as targets of each individual IGF2BP protein, whereas >5,000 mRNAs were being targeted by at least one protein and >2,000 mRNAs were being co-targeted by all three IGF2BPs. The binding sites of IGF2BPs are enriched with m^{6}A motif 'GGAC'. Given that only around 7,000 mRNA transcripts are m^{6}A modified in individual mammalian cells[2,3] and that >80% of IGF2BP targets have at least one m^{6}A peak (Fig. 1g), IGF2BPs probably have a broad impact on m^{6}A-associated gene regulation. Accordingly, reduction of cellular

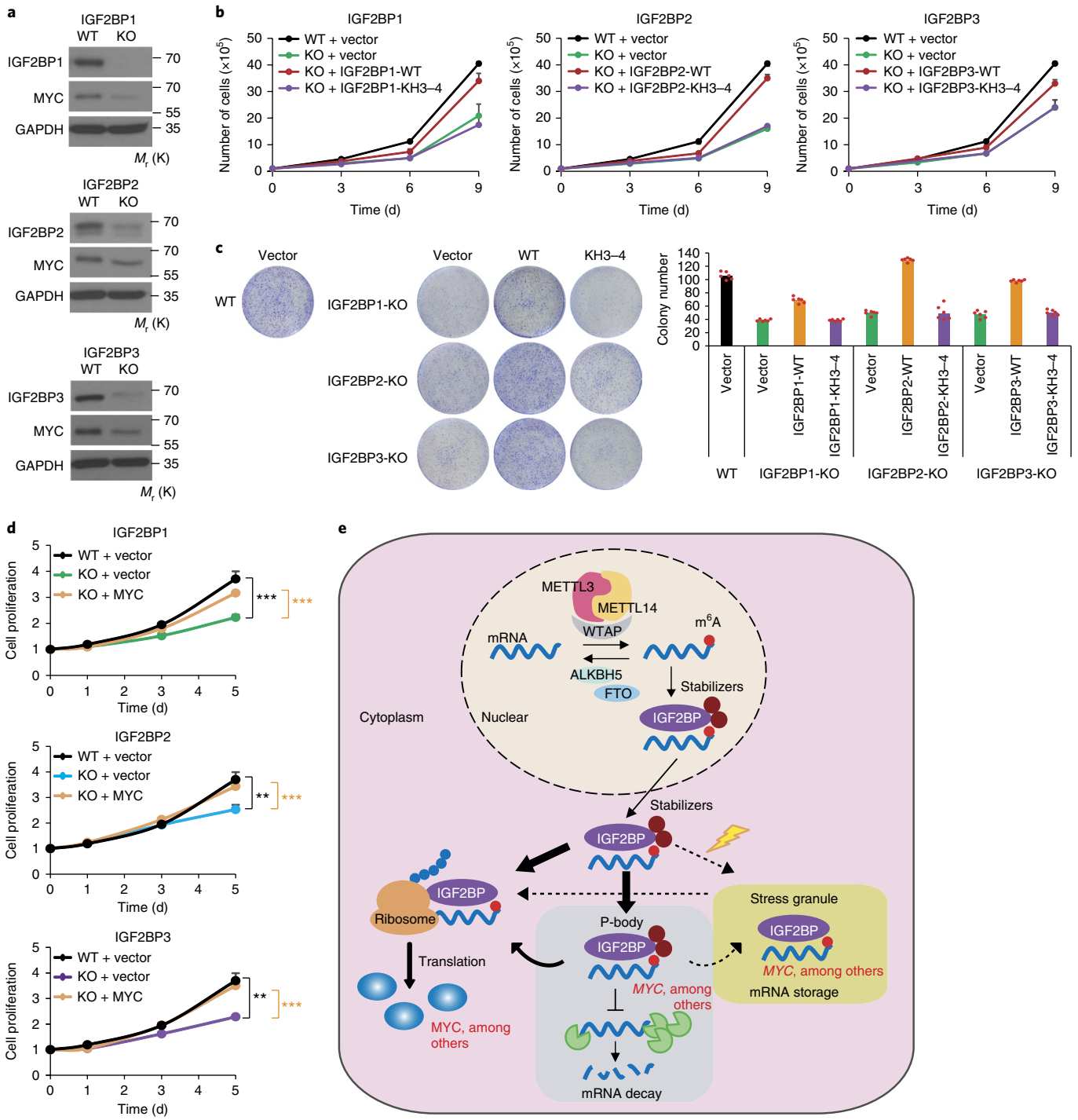

Fig. 7 | IGF2BPs are oncogenic m^{6}A readers. a, CRISPR–Cas9-mediated KO of *IGF2BPs* and the subsequent depletion of MYC in HepG2 cells, as detected by western blotting. Images are representative of three independent experiments. **b**, Effect of wild-type or KH3–4-mutated IGF2BPs on restoring cell proliferation in *IGF2BP*-KO cells. Data shown represent the mean value of viable cell numbers of two independent experiments. **c**, Colony formation assay using wild-type or *IGF2BP*-KO (sgIGF2BP) HepG2 cells. Representative images of crystal violet staining of cells are shown beside the histograms of colony numbers. Colonies were counted from three replicate wells, and two independent experiments were performed. The colony number of each experiment represents the average count of three replicate wells. **d**, MTT assays displaying the effect of MYC on restoring cell proliferation in *IGF2BP*-KO cells. Values are the mean ± s.d. of $n = 3$ independent experiments. Two-tailed student *t*-test were used (**$P < 0.01$; ***$P < 0.001$). **e**, Working model of IGF2BP-mediated regulation of m^{6}A-modified mRNAs. mRNAs were methylated de novo by the methyltransferase complex, which is composed of METTL3, METTL14 and a regulatory subunit WTAP. The naive mRNA with m^{6}A modifications were preferentially recognized by IGF2BP proteins. By recruiting mRNA stabilizers, such as HuR and MATR3, IGF2BPs protect target mRNAs from degradation in the P-body while facilitating translation after being exported to the cytoplasm. Under stress conditions such as heat shock, IGF2BP-containing messenger ribonucleoproteins are translocated to stress granules for the storage of their mRNA targets. ALKBH5, alkB homolog 5 RNA demethylase; FTO, alpha-ketoglutarate dependent dioxygenase FTO. Dashed arrows indicate translocation to or from stress granules. Unprocessed scans of western blot analysis are available in Supplementary Fig. 8. Source data for **b**–**d** are in Supplementary Table 3.

m^{6}A levels upon *METTL14* knockdown impairs the in cellulo binding of FLAG-IGF2BP2/3 to their RNA targets. Furthermore, we demonstrated that IGF2BPs bind directly to *MYC* CRD and promote MYC expression in an m^{6}A-dependent manner.

The direct binding of IGF2BPs to m^{6}A RNAs through their KH domains was demonstrated both in vitro and in cellulo. The KH domain is an evolutionarily conserved RNA recognition element found in several proteins, such as fragile X mental retardation protein 1 (FMR1), heterogeneous nuclear ribonucleoprotein K (HNRPK) and polypyrimidine tract-binding protein 1 (PTBP1)[32]. The KH domains in IGF2BPs were responsible for the recognition and binding of some specific mRNAs, including *ACTIN*, *MYC* and *IGF2* (refs [17,33,34]). Our work reveals a new, m^{6}A-dependent binding mode on top of the primary sequence. We show that the KH domains, especially the KH3–4 di-domain, are critical for the binding of IGF2BPs to m^{6}A-modified RNAs. Nonetheless, KH3–4 peptides alone showed poor selectivity for m^{6}A RNA compared with full-length proteins (data not shown), which is consistent with previous reports that post-translational modifications in the KH3–4 flanking regions may be important for IGF2BP selectivity[17,35]. It is also possible that KH domains are different from the well-defined YTH domains and may not possess discrete pocket for m^{6}A recognition, and that other mechanisms (e.g., reducing solvation penalty, as previously proposed[36]) may be involved in the recognition of m^{6}A by KH domains. Future structural studies are warranted to understand how specific KH domains bind to m^{6}A-modified RNAs. It will also be interesting to investigate other KH domain proteins as potential m^{6}A-binding readers.

Our RNA stability profiling revealed that IGF2BPs stabilize target RNAs. The opposite role of IGF2BPs versus YTHDF2 imposes an additional layer of complexity on m^{6}A function. It is possible that IGF2BPs and YTHDF2 recognize different targets, or compete for the same m^{6}A sites to fine-tune expression of shared targets. In fact, YTHDF2-binding sites show a lower density in the 3′UTRs than in the coding regions[10], which is distinct from IGF2BP-binding sites (Fig. 1h). Analysis of the ENCODE PAR-CLIP data revealed only a very small proportion (0.85–1.20%) of IGF2BP-binding sites being shared by YTHDF2 (Supplementary Fig. 7a). Moreover, a consensus of 'GAAC', in addition to that of 'GGAC', was found from all significant YTHDF2-binding sites (Supplementary Fig. 7b). In addition, we found that IGF2BP-binding sites have a significantly lower guanine–cytosine (GC) content than YTHDF2-binding sites (Supplementary Fig. 7c,d), suggesting that the local nucleotide composition may also contribute to the binding preference of different readers. Together, these data indicate that IGF2BPs and YTHDF2 have a distinct pattern in target recognition and regulation.

The mRNA stabilizing function of IGF2BPs was also supported by its co-factors, HuR and MATR3. In particular, HuR was previously identified as an indirect m^{6}A-binding protein, which increased the stability of bound RNA and blocked microRNA targeting[8,25,37]. Interestingly, we showed here that HuR was co-localized with IGF2BPs in P-bodies, which are locations for mRNA fate decision[38–40]. Our findings suggest that HuR could be recruited by IGF2BPs to protect m^{6}A-containing mRNAs from degradation and facilitate their translation (Fig. 7e). We found that IGF2BPs co-localize with stress granules and shuttle between ribosome and non-ribosome fractions during heat shock and recovery, suggesting a role of IGF2BPs in mRNA translation in stress response. Collectively, IGF2BPs can promote stability by inhibiting mRNA degradation or enhancing mRNA storage under stress, and facilitate their translation (Fig. 7e). We recently reported that METTL14 promotes the stability and translation of *MYC* mRNA and plays an essential oncogenic role in leukaemia[41], which is probably also attributed to IGF2BP-mediated, m^{6}A-dependent regulation of MYC expression.

Dysregulation of IGF2BPs could result in abnormal accumulation of oncogenic products such as MYC, and therefore support the malignant state of cancer cells. Consistent with the frequent amplification of *IGF2BP* genes in various types of cancers, our finding that IGF2BPs exhibit oncogenic roles as m^{6}A readers demonstrates the functional importance of IGF2BPs and their associated m^{6}A reading processes in tumorigenesis, and highlights the therapeutic potential of targeting IGF2BPs in cancers.

Methods

Methods, including statements of data availability and any associated accession codes and references, are available at https://doi.org/10.1038/s41556-018-0045-z.

Received: 23 February 2017; Accepted: 23 January 2018;
Published online: 23 February 2018

References

1. Jia, G. et al. N^6-methyladenosine in nuclear RNA is a major substrate of the obesity-associated FTO. *Nat. Chem. Biol.* **7**, 885–887 (2011).
2. Dominissini, D. et al. Topology of the human and mouse m^{6}A RNA methylomes revealed by m6A-seq. *Nature* **485**, 201–206 (2012).
3. Meyer, K. D. et al. Comprehensive analysis of mRNA methylation reveals enrichment in 3′ UTRs and near stop codons. *Cell* **149**, 1635–1646 (2012).
4. Zhao, X. et al. FTO-dependent demethylation of N^6-methyladenosine regulates mRNA splicing and is required for adipogenesis. *Cell Res.* **24**, 1403–1419 (2014).
5. Su, R. et al. R-2HG exhibits anti-tumor activity by targeting FTO/m6A/MYC/CEBPA signaling. *Cell* **72**, 90–105 (2018).
6. Liu, N. et al. N^6-methyladenosine-dependent RNA structural switches regulate RNA–protein interactions. *Nature* **518**, 560–564 (2015).
7. Geula, S. et al. Stem cells. m^{6}A mRNA methylation facilitates resolution of naive pluripotency toward differentiation. *Science* **347**, 1002–1006 (2015).
8. Wang, Y. et al. N^6-methyladenosine modification destabilizes developmental regulators in embryonic stem cells. *Nat. Cell Biol.* **16**, 191–198 (2014).
9. Chen, T. et al. m^{6}A RNA methylation is regulated by microRNAs and promotes reprogramming to pluripotency. *Cell Stem Cell* **16**, 289–301 (2015).
10. Wang, X. et al. N^6-methyladenosine-dependent regulation of messenger RNA stability. *Nature* **505**, 117–120 (2014).
11. Zhao, B. S., Roundtree, I. A. & He, C. Post-transcriptional gene regulation by mRNA modifications. *Nat. Rev. Mol. Cell Biol.* **18**, 31–42 (2016).
12. Li, Z. et al. FTO plays an oncogenic role in acute myeloid leukemia as a N^6-methyladenosine RNA demethylase. *Cancer Cell* **31**, 127–141 (2017).
13. Zhao, B. S. et al. m^{6}A-dependent maternal mRNA clearance facilitates zebrafish maternal-to-zygotic transition. *Nature* **542**, 475–478 (2017).
14. Wang, X. et al. N^6-methyladenosine modulates messenger RNA translation efficiency. *Cell* **161**, 1388–1399 (2015).
15. Du, H. et al. YTHDF2 destabilizes m^{6}A-containing RNA through direct recruitment of the CCR4–NOT deadenylase complex. *Nat. Commun.* **7**, 12626 (2016).
16. Xiao, W. et al. Nuclear m^{6}A reader YTHDC1 regulates mRNA splicing. *Mol. Cell* **61**, 507–519 (2016).
17. Bell, J. L. et al. Insulin-like growth factor 2 mRNA-binding proteins (IGF2BPs): post-transcriptional drivers of cancer progression? *Cell. Mol. Life Sci.* **70**, 2657–2675 (2013).
18. Nielsen, J. et al. A family of insulin-like growth factor II mRNA-binding proteins represses translation in late development. *Mol. Cell. Biol.* **19**, 1262–1270 (1999).
19. Noubissi, F. K. et al. CRD-BP mediates stabilization of βTrCP1 and c-*myc* mRNA in response to β-catenin signalling. *Nature* **441**, 898–901 (2006).
20. Huttelmaier, S. et al. Spatial regulation of β-actin translation by Src-dependent phosphorylation of ZBP1. *Nature* **438**, 512–515 (2005).
21. Weidensdorfer, D. et al. Control of c-*myc* mRNA stability by IGF2BP1-associated cytoplasmic RNPs. *RNA* **15**, 104–115 (2009).
22. Hafner, M. et al. Transcriptome-wide identification of RNA-binding protein and microRNA target sites by PAR-CLIP. *Cell* **141**, 129–141 (2010).
23. Behm-Ansmant, I., Gatfield, D., Rehwinkel, J., Hilgers, V. & Izaurralde, E. A conserved role for cytoplasmic poly(A)-binding protein 1 (PABPC1) in nonsense-mediated mRNA decay. *EMBO J.* **26**, 1591–1601 (2007).
24. Mangus, D. A., Evans, M. C. & Jacobson, A. Poly(A)-binding proteins: multifunctional scaffolds for the post-transcriptional control of gene expression. *Genome Biol.* **4**, 223 (2003).
25. Fan, X. C. & Steitz, J. A. Overexpression of HuR, a nuclear-cytoplasmic shuttling protein, increases the in vivo stability of ARE-containing mRNAs. *EMBO J.* **17**, 3448–3460 (1998).

26. Salton, M. et al. Matrin 3 binds and stabilizes mRNA. *PLoS ONE* **6**, e23882 (2011).
27. Boudoukha, S., Cuvellier, S. & Polesskaya, A. Role of the RNA-binding protein IMP-2 in muscle cell motility. *Mol. Cell. Biol.* **30**, 5710–5725 (2010).
28. Wachter, K., Kohn, M., Stohr, N. & Huttelmaier, S. Subcellular localization and RNP formation of IGF2BPs (IGF2 mRNA-binding proteins) is modulated by distinct RNA-binding domains. *Biol. Chem.* **394**, 1077–1090 (2013).
29. Stohr, N. et al. ZBP1 regulates mRNA stability during cellular stress. *J. Cell Biol.* **175**, 527–534 (2006).
30. Doyle, G. A. et al. The c-myc coding region determinant-binding protein: a member of a family of KH domain RNA-binding proteins. *Nucleic Acids Res.* **26**, 5036–5044 (1998).
31. Bley, N. et al. Stress granules are dispensable for mRNA stabilization during cellular stress. *Nucleic Acids Res.* **43**, e26 (2015).
32. Valverde, R., Edwards, L. & Regan, L. Structure and function of KH domains. *FEBS J.* **275**, 2712–2726 (2008).
33. Nielsen, J., Kristensen, M. A., Willemoes, M., Nielsen, F. C. & Christiansen, J. Sequential dimerization of human zipcode-binding protein IMP1 on RNA: a cooperative mechanism providing RNP stability. *Nucleic Acids Res.* **32**, 4368–4376 (2004).
34. Chao, J. A. et al. ZBP1 recognition of β-actin zipcode induces RNA looping. *Genes Dev.* **24**, 148–158 (2010).
35. Dai, N. et al. mTOR phosphorylates IMP2 to promote IGF2 mRNA translation by internal ribosomal entry. *Genes Dev.* **25**, 1159–1172 (2011).
36. Roundtree, I. A., Evans, M. E., Pan, T. & He, C. Dynamic RNA modifications in gene expression regulation. *Cell* **169**, 1187–1200 (2017).
37. Peng, S. S., Chen, C. Y., Xu, N. & Shyu, A. B. RNA stabilization by the AU-rich element binding protein, HuR, an ELAV protein. *EMBO J.* **17**, 3461–3470 (1998).
38. Brengues, M., Teixeira, D. & Parker, R. Movement of eukaryotic mRNAs between polysomes and cytoplasmic processing bodies. *Science* **310**, 486–489 (2005).
39. Huch, S. et al. The decapping activator Edc3 and the Q/N-rich domain of Lsm4 function together to enhance mRNA stability and alter mRNA decay pathway dependence in *Saccharomyces cerevisiae*. *Biol. Open* **5**, 1388–1399 (2016).
40. Bett, J. S. et al. The P-body component USP52/PAN2 is a novel regulator of HIF1A mRNA stability. *Biochem. J.* **451**, 185–194 (2013).
41. Weng, H. et al. METTL14 inhibits hematopoietic stem/progenitor differentiation and promotes leukemogenesis via mRNA m^6A modification. *Cell Stem Cell* **22**, 191–205 (2018).

Acknowledgements

We thank the Proteomics Laboratory at the University of Cincinnati for mass spectrometry analysis; the Transgenic Animal and Genome Editing Core at the Cincinnati Children's Hospital Medical Center for design and construction of sgRNA vectors; the Genomics, Epigenomics and Sequencing Core at the University of Cincinnati and the Genomic Facility at the University of Chicago for next-generation sequencing. This work was supported in part by the National Institutes of Health (NIH) R01 grants CA214965 (J.C.), CA211614 (J.C.), CA178454 (J.C.), CA182528 (J.C.), CA163493 (J.-L.G.), RM1 HG008935 (C.He), 1S10RR027015-01 (K.D.G.) and grants 2017YFA0504400 (J.Y.), 91440110 (J.Y.) and 31671349 (L.Q.) from the National Nature Science Foundation of China. J.C. is a Leukemia & Lymphoma Society (LLS) Scholar. C.He is an investigator of the Howard Hughes Medical Institute (HHMI). B.S.Z. is an HHMI International Student Research Fellow.

Author contributions

H.H., H.Weng and J.C. conceived and designed the entire project. H.H., H.Weng, C.He, J.Y. and J.C. designed and supervised the research. H.H., H.Weng, X.Q., H.S., H.Wu, B.S.Z., A.M., C.Liu, C.L.Y., J.R.S., R.S., X.D., M.S., C.Li, S.N., Y.W., C.Hu, K.F. and J.C. performed the experiments and/or data analyses. H.H., H.Weng, W.S., L.D. and J.Y. performed the genome-wide or transcriptome-wide data analyses. Y.-C.H., S.H., K.D.G., X.J., M.W., L.Q., J.-L.G., C.He, J.Y. and J.C. contributed reagents/analytic tools and/or grant support. H.H., H.Weng, W.S., H.S., B.S.Z., A.M., S.N., C.He, J.Y. and J.C. wrote and revised the paper. All authors discussed the results and commented on the manuscript.

Competing interests

C.He is a scientific founder of Accent Therapeutics, Inc.

Additional information

Supplementary information is available for this paper at https://doi.org/10.1038/s41556-018-0045-z.

Reprints and permissions information is available at www.nature.com/reprints.

Correspondence and requests for materials should be addressed to C.H. or J.Y. or J.C.

Publisher's note: Springer Nature remains neutral with regard to jurisdictional claims in published maps and institutional affiliations.

Methods

Plasmids and short interfering RNAs. pcDNA3-based vectors encoding wild-type and KH domain mutant FLAG-tagged chicken ZBP1 (refer to as IGF2BP1), human IGF2BP2 and IGF2BP3 were kindly provided by Dr Hüttelmaier (Martin Luther University, Germany). RRM domain truncation of IGF2BP2 (IGF2BP2-ΔRRM) was produced by PCR using the Q5 Site Directed Mutagenesis Kit (NEB) with forward primer 5′-GAAGAGGTGAGCTCCCCT-3′ and reverse primer 5′-GAATTCCTTGTCGTCGTCC-3′. The plasmid encoding human MYC (pCDNA3-HA-HA-humanCMYC) was obtained from Addgene. The RNAi Consortium (TRC) lentiviral vectors encoding shRNAs against IGF2BP1 (TRCN0000075149 and TRCN0000075152), IGF2BP2 (TRCN0000149002 and TRCN0000148565), IGF2BP3(TRCN0000074677 and TRCN0000074673), METTL3 (TRCN0000034715), METTL14 (TRCN0000015933) and their non-specific control (shNS, RHS6848) were purchased from GE Dharmacon, whereas the packing vectors, pMD2.G, pMDLg/pRRE and pRSV-Rev, were obtained from Addgene. The MYC short interfering RNA (siRNA) was purchased from Santa Cruz Biotechnology, whereas the HuR siRNA was from GE Dharmacon.

Cell culture and transfection. The human hepatocellular carcinoma cell line HepG2 (ATCC HB-8065) was maintained in EMEM medium (American Type Culture Collection (ATCC)) supplemented with 10% FBS (Invitrogen), 2 mM L-glutamine and 1% penicillin–streptomycin. HEK293T and HeLa cells were grown in DMEM medium (Invitrogen) containing 10% FBS, 2 mM L-glutamine and 1% penicillin–streptomycin. All cell lines were purchased from the ATCC and were not authenticated by ourselves. All cell lines were routinely tested for mycoplasma contamination. These cell lines were not listed in the database of commonly misidentified cell lines maintained by the International Cell Line Authentication Committee (ICLAC). For heat-shock treatment, HeLa cells were incubated at 42 °C for 1 h. Plasmids and siRNAs were transfected into cells with Lipofectamine 2000 (Invitrogen) according to the manufacturer's instructions.

Isolation and lentiviral infection of CD34⁺ cells. Cord blood of healthy donors was obtained from Cincinnati Children's Hospital Medical Center (CCHMC, Ohio, USA) and subjected to isolation of mononuclear cells using Ficoll-Paque PLUS (GE Healthcare Life Sciences). Human CD34⁺ haematopoietic stem/progenitor cells were then purified from mononuclear cells by using human CD34 MicroBead Kit (Miltenyi Biotec). The CD34⁺ cells were cultured in StemSpan SFEM medium (StemCell Technologies) supplemented with 1% Lipid Mixture 1 (L0288, Sigma-Aldrich), 2 mmol per litre L-glutamine, 1% penicillin–streptomycin, 100 ng per ml stem cell factor (SCF), and 2 ng per ml IL-3. Cells were infected with concentrated lentiviral particles through two rounds of 'spinoculation'.

RNA affinity chromatography and nLC-ESI-MS/MS. Biotin-labelled RNA oligonucleotides containing adenosine or m⁶A were synthesized by GE Dharmacon. The hpRNA baits were denatured at 99 °C for 10 min and slowly cooled down to room temperature to allow the formation of stem-loop structure before use. The single-stranded RNA baits were denatured at 99 °C for 10 min and put on ice immediately, unless otherwise specified. Each RNA oligonucleotide (0.4 pmol, unless otherwise specified) was immobilized onto 50 µl streptavidin magnetic beads (Thermo Fisher Scientific) in binding buffer (20 mM Tris, 200 mM NaCl, 6 mM EDTA, 5 mM potassium fluoride, 5 mM β-glycerophosphate, 2 µg per ml aprotinin at pH 7.5) at 4 °C for 4 h. RNA bait-conjugated streptavidin beads were then incubated with 200 µg of HEK293T nuclear extract or 0.5–1 ug of human recombinant proteins in binding buffer in a final volume of 400 µl overnight at 4 °C. After extensive washing, RNA–protein complexes were dissolved in 1× SDS buffer, separated under denaturing conditions on 10% SDS-polyacrylamide Bis-Tris gels and detected by silver staining (Thermo Fisher Scientific) or western blot analysis. For mass spectrometry analysis, proteins in gel slices were digested with trypsin. The recovered peptides were introduced into an Eksigent nanoLC.ultra nanoflow system attached to a TripleTOF 5600 plus (Sciex) for nano-liquid chromatography-coupled electrospray ionization multistage tandem mass spectrometry (nLC-ESI-MS/MS) analyses.

Protein expression and purification. FLAG-tagged IGF2BP1, IGF2BP2 and IGF2BP3 were expressed in HEK293T cells. For each protein, four 15-cm dishes of cells were prepared and lysed in 4 ml lysis buffer (50 mM Tris-HCl pH 7.5, 300 mM KCl, 0.5% NP-40, 5% glycerol, 5 µg per ml DNase I, 1% RNase T1/A, 1% protease inhibitor, 1 mM dithiothreitol) at 4 °C for 1 h and sonicated (5 s on, 25 s off, for 24 cycles). The lysate was then cleared by centrifuge at 4 °C. The proteins were affinity purified using 40 µl anti-FLAG M2 resin (Sigma-Aldrich) at 4 °C for 2 h. After extensive wash with wash buffer (50 mM Tris-HCl, pH 7.5, 300 mM KCl, 5% glycerol, 1 mM dithiothreitol), proteins were eluted in 500 µl 1× FLAG elution solution (0.5 mg per ml FLAG peptide in wash buffer) at 4 °C for 1 h. Protein purity was verified with SDS–PAGE followed by coomassie staining.

Electrophoretic mobility shift assay/gel shift assay. The Cy5.5-labelled RNA oligonucleotides (ss-A: Cy5.5-CGUCUCGGACUCGGACUGCU; ss-m6A: Cy5.5-CGUCUCGG(m6A)CUCGG(m6A)CUGCU) with the same sequences of biotin-labelled ss-A and ss-m⁶A were synthesized by GE Dharmacon. The gel shift assay was performed as previously described[10]. Briefly, RNA probes were denatured by heating at 65 °C for 5 min and slowly cooling down to room temperature. For each reaction, 1 µl RNA probes (4 nM final concentration) and 1 µl protein (10× of the concentration gradient indicated in Supplementary Fig. 1d) were incubated in 8 µl binding buffer (10 mM Tris-HCl pH 7.5, 50 mM KCl, 1 mM EDTA, 0.05% Triton X-100, 5% glycerol, 1 mM dithiothreitol and 40 U per ml RNasin) on ice for 30 min. The RNA–protein mixtures were separated in 5% native polyacrylamide gels (in 0.5× Tris-borate-EDTA buffer) at 4 °C for 60 min at 13 V per cm. The fluorescence signal was visualized by Odyssey Imaging Systems (LI-COR Biosciences) and quantified by ImageMaster TotalLab (GE Healthcare). The dissociation constant (K_d) was calculated with non-linear curve fitting (function one site-specific binding) using GraphPad Prism with $y = B_{max}*x/(K_d + x)$, where y is the ratio of [RNA–protein]/([free RNA] + [RNA–protein]), x is the input protein concentration, and B_{max} is set to 1.

m⁶A dot blot. The m⁶A dot blot assay was conducted as previously described[12]. Briefly, the indicated amount of total cellular RNA or synthesized RNA oligonucleotide was denatured in 3-fold volume of RNA incubation buffer (65.7% fomamide, 7.77% formaldehyde and 1.33× MOPS) at 65 °C for 5 min, followed by chilling on ice and mixing with 1-fold volume of 20× SSC. RNA samples were applied to Amersham Hybond-N + membrane (GE Healthcare) with a Bio-Dot Apparatus (BioRad). After UV crosslinking, the membrane was stained with 0.02% methylene blue in 0.3 M sodium acetate. The membrane was then washed with 1× PBST buffer, blocked with 5% non-fat milk in PBST, and incubated with anti-m⁶A antibody (202003, 1:1,000; Synaptic Systems) overnight at 4 °C. After incubating with horseradish peroxidase-conjugated anti-rabbit IgG secondary antibody (Santa Cruz Biotechnology), the membrane was visualized using Amersham ECL Prime Western Blotting Detection Reagent (GE Healthcare).

Western blotting. Cells were lysed using 1× SDS buffer and sonicated. Equal amounts of proteins were loaded and separated by 10% SDS–PAGE, transferred to polyvinylidene fluoride membranes, and detected by immunoblotting with the Pierce ECL Western Blotting Substrate (Thermo Fisher Scientific) or Amersham ECL Prime Western Blotting Detection Reagent. Antibodies used for western blotting were as follows unless otherwise specified: IGF2BP1 (IMP1, clone D33A2, no. 8482), IGF2BP2 (IMP2, clone D4R2F, no. 14672), MYC (clone D3N8F, no. 13987), HuR (ELAVL1, clone D9W7E, no. 12582) were from Cell Signaling Technology (CST), IGF2BP3 (IMP3, A303-426A) and MATR3 (A300-591A-T) were from Bethyl Laboratories, and FLAG (M2, F3165) was from Sigma-Aldrich. GAPDH (sc-47724, Santa Cruz) was used as a loading control.

Prediction of m⁶A-binding proteins. We developed a computational pipeline to discover the potential m⁶A-binding proteins from ENCODE and published RBP-CLIP data sets generated by various CLIP methods, including high-throughput sequencing of RNA isolated by CLIP (HITS-CLIP), PAR-CLIP, eCLIP, individual-nucleotide resolution CLIP (iCLIP) and infrared-CLIP (irCLIP). The CLIP–seq peaks of each RBP were intersected with known m⁶A sites[42] to calculate the ratio between the number of peaks overlapping with m⁶A-peak sites and the total number of peaks (m⁶A-containing peak number/total peak number). These peaks were imported into HOMER software[43] for de novo motif identification. The potential m⁶A-binding proteins should meet the following requirements: (1) the ratio (m⁶A-containing peak number/total peak number) should be >10%; and (2) for the identified motifs of each RBP, the P value should be $<1\times10^{-35}$. Based on this pipeline, all the top de novo motifs could be identified unbiasedly. Nevertheless, because we are interested in the identification of m⁶A-binding proteins, we further focused on the proteins that have top motifs containing 'GGAC', which represents the most common m⁶A consensus sequence.

LC-MS/MS. 50–100 ng of mRNA were digested by nuclease P1 (1U, Wako Pure Chemical) in 25 µl of buffer containing 20 mM of NH_4OAc (pH 5.3) at 42 °C for 2 h, followed by the addition of NH_4HCO_3 (1 M, 3 µl, freshly made) and alkaline phosphatase (1 U, Sigma). After an additional incubation at 37 °C for 2 h, the sample was diluted to 50 µl and filtered (0.22 µm pore size, 4 mm diameter, Millipore), and 5 µl of the solution was injected into LC-MS/MS. Nucleosides were separated by reverse-phase ultra-performance liquid chromatography on a C18 column with on-line mass spectrometry detection using an Agilent 6410 QQQ triple-quadrupole LC mass spectrometer in positive electrospray ionization mode. The nucleosides were quantified by using retention time and the nucleoside to base ion mass transitions of 284–152 (G), 282.1–150.1 (m⁶A), 268–136 (A), 245–113.1 (U) and 244–112 (C). Quantification was performed in comparison with the standard curve obtained from pure nucleoside standards running with the same batch of samples. The m⁶A level was calculated as the ratio of m⁶A to A or the ratio of m⁶A to (A + U + C + G) based on the calibrated concentrations.

RIP-LC-MS/MS. The RIP procedure was reported previously[10]. Three 15-cm dishes of confluent HEK293T cells transiently overexpressing FLAG-tagged IGF2BP (1, 2 or 3) were subjected to the RIP procedure. Input, flow-through and IGF2BP-bound RNA were purified with TRIzol reagent (Invitrogen). mRNA from the three portions was further purified by depleting ribosomal RNA (rRNA)

with RiboMinus Eukaryote Kit v2 (Ambion) followed by depleting transfer RNA (tRNA) with RNA Clean and Concentrator-5 (Zymo Research). 50 ng purified mRNA of each sample was subjected to LC-MS/MS quantification of m^{6}A levels as reported previously[10].

RIP. RIP was performed as previously described[44] with some modifications. Briefly, cells seeded in a 10-cm dish at 70–80% confluency were crosslinked by UV and harvested by trypsinization. Nuclear extraction was isolated and sonicated. 1 µg of FLAG (F3165, Sigma-Aldrich), IGF2BP1 (8482, CST) or IGF2BP2 (14672, CST) antibody or a corresponding control IgG (mouse IgG (CS200621, Millipore) for FLAG, rabbit IgG (NI01, Millipore) for IGF2BP1 and IGF2BP2) was conjugated to protein A/G magnetic beads (Thermo Fisher Scientific) by incubation for 4 h at 4 °C, followed by washing three times and incubation with pre-cleared nuclear extraction in RIP buffer (150 mM KCl, 25 mM Tris (pH 7.4), 5 mM EDTA, 0.5 mM DTT, 0.5% NP40, 1× protease inhibitor) at 4 °C overnight. After washing with RIP buffer for three times, beads were resuspended in 80 µl PBS, followed by DNA digestion at 37 °C for 15 min and incubation with 50 µg of proteinase K (Thermo Fisher) at 37 °C for 15 min. Input and co-immunoprecipitated RNAs were recovered by TRIzol, extraction and analysed by qPCR or RNA-seq.

CLIP. CLIP was performed following previously reported protocol[10] with some modifications. HEK293T cells seeded in four 15-cm plates at approximately 80% confluency were treated with 200 µM 4-thiouridine. After 16 h, cells were washed with ice-cold PBS, crosslinked with 150 mJ per cm^2 of 365 nm UV light and harvested by trypsinization. Nuclear extraction was isolated and sonicated. 2–3 mg of nuclear lysates were serially digested by 0.05 U per µl DNase RQ1 at 37 °C for 5 min, and 0.2 U per µl RNase T1 at 22 °C for 15 min. 10 µg of FLAG (F3165, Sigma-Aldrich) or IGF2BP2 (14672, CST) antibody was conjugated to protein A/G magnetic beads and incubated with nuclear lysates in RIP buffer at 4 °C overnight. After washing with RIP buffer for three times, a second round of RNase T1 digestion was conducted under 50 U per µl at 22 °C for 15 min. Input and immunoprecipitated RNAs were recovered and analysed by qPCR.

RNA-seq. Total RNA was isolated from IGF2BP knockdown or control HepG2 cells using miRNeasy Kit (Qiagen). Poly(A) RNA was subsequently purified from 50–100 ng total RNA using NEBNext Poly(A) mRNA Magnetic Isolation Module. NEBNext Ultra Directional RNA Library Prep Kit (New England BioLabs) was used for library preparation. Each group was sequenced in triplicate.

RNA stability assay and sequencing for mRNA lifetime. HepG2 cells with stably expressed shRNAs against IGF2BPs or shNS were seeded into 6-well plates to get 50% confluency after 24 h. Cells were treated with 5 µg per ml actinomycin D and collected at indicated time points. The total RNA was extracted by miRNeasy Kit (Qiagen) and analysed by RT–PCR and RNA-seq. For RNA-seq, an equal amount of external RNA control consortium (ERCC) RNA spike-in control (Thermo Fisher Scientific) was added to the total RNA samples as internal controls before library construction. Sequencing libraries were prepared using NEBNext Ultra Directional RNA Library Prep Kit. RNA stability profiling was generated from two biological replicates.

The turnover rate and half-life of mRNA was estimated according to a previously published paper[45]. As actinomycin D treatment results in transcription stalling, the change of mRNA concentration at a given time (dC/dt) is proportional to the constant of mRNA decay (K_{decay}) and the mRNA concentration (C), leading to the following equation:

$$dC/dt = -K_{decay}C$$

Thus, the mRNA degradation rate K_{decay} was estimated by:

$$\ln(C / C_0) = -K_{decay}t$$

To calculate the mRNA half-life ($t_{1/2}$), when 50% of the mRNA is decayed (that is, $C/C_0 = 1/2$), the equation was:

$$\ln(1 / 2) = -K_{decay}t_{1/2}$$

From where:

$$t_{1/2} = \ln 2 / K_{decay}$$

m^{6}A-seq. Total RNA was extracted by homogenizing cells in TRIzol reagent and purifying with Direct-zol RNA MiniPrep kit (Zymo). mRNA was further purified using Dynabeads mRNA Purification Kit (Thermo Fisher). RNA fragmentation was performed by sonication at 10 ng per µl in 100 µl RNase-free water using Bioruptor Pico (Diagenode) with 30 s on and 30 s off for 30 cycles. m6A-immunoprecipitation and library preparation were performed according to published protocol[2]. Sequencing was carried out on Illumina HiSeq 2000 according to the manufacturer's instructions.

Sequencing data analysis. For RIP–seq data: samples were sequenced by Illumina HiSeq 1000 with a single-end 51-base pair (bp) read length. The RIP–seq reads were mapped to human genome version hg19 by Tophat2 version 2.0.13 with default settings[46]. Differential gene expression was calculated by Cuffdiff version v2.2.1 (ref. [47]). The RIP targets were defined as genes with reads per kilobase, per million reads (RPKM) ≥ 1, immunoprecipitation/input ≥ 2, and $P < 0.05$.

For PAR-CLIP data: The IGF2BPs PAR-CLIP data were obtained from the public database Gene Expression Omnibus (GEO; accession No. GSE21918)[22]. The adapters were trimmed by using cutadapt version 1.9.1 (ref. [48]). The processed reads were mapped to human genome version hg19 by bowtie version 1.1.2 with parameters: –v 3 –m 5 --best --strata[49]. The mapped results were analysed by PARalyzer v1.5 with default settings[50]. The results were further filtered by ModeScore ≥ 0.6. For peaks that were larger than 50 nt, we extracted 50 nt centered on the ModeLocation site. GENCODE v24 was used to annotate the filtered peaks, and finally, the PAR-CLIP target genes of IGF2BP1 (7511), IGF2BP2 (7974) and IGF2BP3 (9228) were identified. We then chose peaks that overlapped with RIP targets for de novo motif analysis using HOMER software with default RNA analysis parameters.

For eCLIP data: to identify IGF2BP footprints, all mapped reads to consecutive genomic peaks were first assembled. Significant peaks were calculated by determining the read-number cutoffs using the Poisson distribution as previously described[51]. The Poisson distribution assumes all intervals are independent and have equal probability of an occurrence happening. Peaks with significantly high read-number values ($P < 10 \times 10^{-5}$ and the minimum peak height ≥ 10) and occurring in both biological duplicates were defined as IGF2BP footprints. We performed de novo motif identifications on eCLIP peaks using the HOMER software[43] with default RNA analysis parameters.

For RNA-seq data: all RNA-seq samples were sequenced by Illumina HiSeq 1000 with single-end 51-bp read length. All reads were mapped to human genome version hg19 by hisat2 v2.0.4 with default settings[52]. Read counts were calculated using HTSeq[53], and was converted to RPKM using our custom Perl script. The average gene expression values of three independent studies were used for the following analysis.

For mRNA lifetime profiling: all RNA-seq samples for mRNA lifetime profiling were sequenced by Illumina HiSeq1000 with single-end 51-bp read length. All reads were mapped to human genome version hg19 by hisat2 v2.0.4 with default settings[52]. Read counts were calculated using HTSeq[53], and was converted to RPKM by our custom Perl script. RPKM was converted to attomole by linear fitting of the RNA spike-in as previously described[10]. The degradation rate of RNA and the mRNA half-life were calculated according to the aforementioned formula. The final half-life was calculated by using the average value of 1 h, 3 h and 6 h.

For m^{6}A-seq: samples were sequenced by Illumina HiSeq 2000 with single-end 50-bp read length. All reads were mapped to human genome version hg19 by tophat v2.0.13 with default settings[46]. The m^{6}A level changes for shMETTL14/shNS were calculated by using exomePeak[54]. Gene expression level changes for input and treatment were analysed using Cuffdiff.

Integrative data analysis and statistics. Three biological replicates of RNA-seq were conducted for shNS, shIGF2BP1, shIGF2BP2 and shIGF2BP3. The genes expression values used were the average of the three replicates. The differential expression patterns of non-targets, PAR-CLIP targets and CLIP + RIP targets were compared for each IGF2BP isoform by $\log_2$ transformed FC (that is, $\log_2$(shIGF2BP1/shNS), $\log_2$(shIGF2BP2/shNS) and $\log_2$(shIGF2BP3/shNS)). Non-parametric Mann–Whitney U-test (Wilcoxon rank-sum test, two-sided, significance level = 0.05) was applied for calculating the P value[10]. The same analysis was applied for mRNA half-life.

Gene-specific m^{6}A qPCR. m^{6}A modifications on individual genes were determined using Magna MeRIP m^{6}A Kit (Millipore) following the manufacturer's instructions. Briefly, 100 µg of total RNA was sheared to about 100 nt in length by metal-ion-induced fragmentation, then purified and incubated with anti-m^{6}A antibody (202003, Synaptic Systems)-conjugated or mouse IgG (CS200621, Millipore)-conjugated beads in 500 µl 1× immunoprecipitation buffer supplemented with RNase inhibitors at 4 °C overnight. Methylated RNA was immunoprecipitated with beads, eluted by competition with free m^{6}A, and recovered with RNeasy kit (Qiagen). One-tenth of the fragmented RNA was saved as input control, and further analysed by qPCR along with MeRIPed RNA. The related enrichment of m^{6}A in each sample was calculated by normalizing to tenfold input.

Immunofluorescence and microscopy. HeLa cells were grown on cover slides, fixed and stained with indicated antibodies as previously described[55]. Antibodies used for immunofluorescence were as follows: FLAG (F3165, 1:200, Sigma-Aldrich), HuR (12582, 1:200, CST), DCP1A (A303-590A-T, 1:200, Bethyl Laboratories), Alexa Fluor 488 anti-rabbit IgG (4412, 1:500, CST), Alexa Fluor 594 anti-mouse IgG (8890, 1:500, CST). Nuclei were stained by 4,6-diamidino-2-phenylindole (DAPI). Image acquisition was performed on a Zeiss LSM-710 confocal microscope under a ×63 oil objective (Zeiss).

Polysome profiling. We followed the procedure reported previously[14] with the following modifications. We started with one 15-cm dish of confluent HEK293T cells transiently overexpressing FLAG-tagged IGF2BP (1, 2 or 3) or infected with lentiviral shRNA targeting IGF2BP1. Before collection, cycloheximide was added to the media at 100 µg per ml for 7 min. The lysis buffer was formulated as 20 mM HEPES, pH 7.6, 100 mM KCl, 5 mM $MgCl_2$, 100 µg per ml cycloheximide, 1% Triton X-100, freshly added 1:100 protease inhibitor (Roche), 40 U per ml SUPERasin (Ambion). The sample was then fractioned into 30 fractions, 0.5 ml per fraction, and analysed by Gradient Station (BioCamp) equipped with ECONOUV monitor (BioRad) and Gilson FC203B fraction collector (Mandel Scientific). Sample from each fraction was subjected to western blot analysis for FLAG (A5892, Sigma-Aldrich), eIF3A (3411, CST), eIF3B (sc-16377, Santa Cruz) and HuR (A-21277, Molecular Probes), or to qPCR analysis of the *MYC* transcript.

For detection of endogenous IGF2BP proteins in ribosomal fractions, three 15-cm dishes of HepG2 cells at approximately 80% confluency were harvested as described above. Sample from each fraction was subjected to western blot analysis for IGF2BP1, IGF2BP2 and IGF2BP3.

Dual-luciferase reporter assay. To generate the CRD firefly luciferase reporter construct, DNA fragments of wild-type and mutant CRD were synthesized by Integrated DNA Technologies and cloned into the XhoI site of the pMIR-REPORT vector (Ambion). HEK293T or HeLa cells were seeded in triplicate in 24-well plates to allow 70% confluency in the next day. 100 ng reporter plasmids with wild-type or mutant CRD (pMIR-CRD1-WT and pMIR-CRD-mut, respectively) and 20 ng renilla luciferase (Rluc) control plasmids (pRL-TK) were co-transfected with or without IGF2BPs expression vectors using Lipofactamine 2000 (Invitrogen). Fluc and Rluc activities were measured 24-h later with the Dual-Luciferase Reporter Assay System (Promega) according to the supplier's instructions. The relative luciferase activity was calculated by dividing Fluc by Rluc and normalized to individual control for each assay. For measuring *Fluc* mRNA changes, lysates left from luciferase activity measurement were lysed with Qiazol reagent and total RNAs were extracted for qPCR analysis of *Fluc* and *Rluc* mRNA abundance. The relative luciferase mRNA was calculated as described above.

Protein co-immunoprecipitation and nLC-ESI-MS/MS. Cells grown in 10-cm dishes at 70–80% confluency were lysed with 500 µl NP40 buffer (150 mM NaCl, 1.5 mM $MgCl_2$, 0.5% NP40, 50 mM Tris-HCl at pH 8.0) and sonicated. Proteins were immunoprecipitated from 500 µg of cell lysates with FLAG or IGF2BP1 antibody and the corresponding IgG (as described above). After applying a magnet, proteins associated with Protein A/G Magnetic Beads were washed three times and analysed by western blotting.

For mass spectrometry analysis, the protein complexes were eluted from beads by incubation with 0.2 mol per litre glycine buffer (pH 2.6), followed by neutralization with equal volume of 1 mol per litre Tris pH 8.0, and identified using nLC-MS/MS by the Proteomics Laboratory (University of Cincinnati, Ohio, USA). Briefly, samples from immuno-enrichment with IgG and FLAG antibodies were solubilized in Laemmli gel buffer and loaded onto separated lanes of a 4–12% MOPS mini SDS polyacrylamide gel, then electrophoresed for 15 min. The entire gel region containing the proteins was cut from the gel and subjected to in-gel trypsin digestion and subsequent recovery of peptides as described previously[56]. The recovered peptides were introduced into an Eksigent nanoLC.ultra nanoflow system attached to a TripleTOF 5600 plus (Sciex) for nLC-ESI-MS/MS analyses. Data were recorded using Analyst-TF (v1.7) software. Searches from the nLC-MS/MS were accomplished using ProteinPilot software (v5.0, revision 4769) that utilizes Paragon algorithm (v5.0.0.0, 4769) against the complete database of homo sapiens protein (20,342 proteins) downloaded from ftp.uniprot.org on 21 January 2016.

Lentiviral shRNA infection. Lentiviruses were produced in HEK293T cells by co-transfecting individual shRNA construct with packing vectors (pMD2.G, pMDLg/pRRE and pRSV-Rev) into HEK293T cells in a 60-mm cell culture dish using X-tremeGENE HP DNA Transfection Reagent (Roche Diagnostics). The lentivirus particles were harvested at 48 h and 72 h after transfection and directly added into target cells with 4 µg per ml polybrene. After two rounds of infection, cells were selected for at least two passages by adding 1 µg per ml puromycin into growth medium.

Cell proliferation, migration and invasion assays. HeLa and HepG2 cells were seeded in 96-well plates at 1,000 cells per well. Cell proliferation was evaluated by MTT Assay (Promega).

For the colony formation assay, 2,000 HeLa cells or 10,000 HepG2 cells were seeded in 6-well plates and stained with crystal violet 7–10-days later. Colonies were counted in three random fields under a ×5 microscope.

For the cell migration and invasion transwell assays, 25,000 HepG2 cells or 50,000 HeLa cells in 500 µl starvation media were plated on the top chambers of Transwell Clear Polyester Membrane Inserts (for the migration assay, Corning Costar) and BioCoat Matrigel Invasion Chambers (for the invasion assay, Corning Costar), while culture media with 20% FBS was applied on the bottom. After 48–72 h, migrated or invaded cells were stained with crystal violet and counted under a ×20 microscope.

For the wound-healing assay, HeLa and HepG2 cells were seeded in 24-well plates and allowed to grow to confluent monolayer in 24 h. Cells were then scratched and allowed to continue to culture in complete culture media to allow for migration for 24–72 h. Images were taken at the indicated time under microscope. The scratched areas were quantified using Adobe Photoshop and were used to calculate migration rate.

RNA isolation and quantitative RT–PCR. Total RNA was isolated from cultured cells using miRNeasy Kit or TRIzol reagent. First-strand complementary DNA (cDNA) was synthesized by reverse transcription of 500 ng RNA using QuantiTect Reverse Transcription Kit (Qiagen). qPCR was carried out using QuantiTect SYBR Green PCR Kit (Qiagen) and mRNA expression was normalized to reference genes, GAPDH and TATA-binding protein (TBP). The primers used in all qPCR assays are listed in Supplementary Table 2.

CRISPR–CSP9 KO. Human HepG2 cells were transiently transfected with a modified pSpCas9(BB)-2A-GFP plasmids (48138, Addgene) containing IGF2BP1, IGF2BP2 or IGF2BP3 single-guide RNAs (sgRNAs) with optimized scaffold[57] and a high-fidelity eSpCas9(1.1)[58] using Lipofectamine 2000 (Invitrogen) following the manufacturer's instructions. Single cells were isolated 48 h after transfection by FACS (BD FACS Aria III) into 96-well plates. Only cells with high levels of green fluorescent protein (GFP; top 4%) were selected. Independent clones were allowed to grow for 3 weeks. KO efficiency was tested by western blotting with specific antibodies. The sgRNA sequences used are listed below: IGF2BP1, TATTCCACCCCAGCTCCGAT; IGF2BP2, GAGAAGTGCCCCCAGGGGCG; IGF2BP3, TGGCACCGACTGATAGAGCT.

Statistics and reproducibility. Statistical comparisons were performed by using *t*-tests (two-tailed) or Wilcoxon and Mann–Whitney test as indicated in the figure legends. Data are presented as mean ± s.d. $P < 0.05$ was considered significant. The number of biological (non-technical) replicates for each experiment is indicated in the figure legends. Three independent sets of RNA samples were used for RNA-seq, two independent sets of RNA samples were used for mRNA stability profiling and two sets of RNA samples were used for m^6A-seq. All western blot, dot blot and immunofluorescence images are representative of three independent experiments. No statistical method was used to predetermine sample size.

Life Sciences Reporting Summary. Further information on experimental design is available in the Life Sciences Reporting Summary.

Code availability. The custom Perl and R scripts used in this study are available on request to the corresponding authors.

Data availability. All sequencing data that support the findings of this study have been deposited in NCBI's GEO under accession number GSE90639 (for RIP–seq), GES90642 (for m^6A-seq), and GSE90684 (for RNA-seq). Data for LC/MS/MS of IGF2BP2 co-immunoprecipitation have been deposited to Figshare (https://doi.org/10.6084/m9.figshare.5693410). Previously published ENCODE PAR-CLIP and eCLIP data that were re-analysed here are available under accession code: GSE21918 (for PAR-CLIP of IGF2BPs), GSE92021 (for IGF2BP1 eCLIP in HepG2), GSE92220 (for IGF2BP3 eCLIP in HepG2) and GSE78509 (for IGF2BPs eCLIP in hESCs).The human cancer data were derived from TCGA Research Network (http://cancergenome.nih.gov/). The data set derived from this resource that supports the findings of this study is available in the cBioPortal for Cancer Genomics (http://www.cbioportal.org/, using TCGA pan-cancer studies).

Source data for Figs. 1c,k, 2c,f, 3d,e, 4b–d,f–j, 5d–f, 6b–d and 7b–d and Supplementary Figs. 2e, 3d–f, 4c, 5a,d and 6d,f–j are provided in Supplementary Table 3. All other data supporting the findings of this study are available from the corresponding authors on reasonable request.

References

42. Sun, W. J. et al. RMBase: a resource for decoding the landscape of RNA modifications from high-throughput sequencing data. *Nucleic Acids Res.* **44**, 259–265 (2016).
43. Heinz, S. et al. Simple combinations of lineage-determining transcription factors prime *cis*-regulatory elements required for macrophage and B cell identities. *Mol. Cell* **38**, 576–589 (2010).
44. Rinn, J. L. et al. Functional demarcation of active and silent chromatin domains in human HOX loci by noncoding RNAs. *Cell* **129**, 1311–1323 (2007).
45. Chen, C. Y. A., Ezzeddine, N. & Shyu, A. B. Messenger RNA half-life measurements in mammalian cells. *Methods Enzymol.* **448**, 335–357 (2008).
46. Kim, D. et al. TopHat2: accurate alignment of transcriptomes in the presence of insertions, deletions and gene fusions. *Genome Biol.* **14**, R36 (2013).
47. Trapnell, C. et al. Transcript assembly and quantification by RNA-seq reveals unannotated transcripts and isoform switching during cell differentiation. *Nat. Biotechnol.* **28**, 511–515 (2010).

48. Martin, M. Cutadapt removes adapter sequences from high-throughput sequencing reads. *EMBnet. J.* **17**, 10–12 (2011).
49. Langmead, B., Trapnell, C., Pop, M. & Salzberg, S. L. Ultrafast and memory-efficient alignment of short DNA sequences to the human genome. *Genome Biol.* **10**, R25 (2009).
50. Corcoran, D. L. et al. PARalyzer: definition of RNA binding sites from PAR-CLIP short-read sequence data. *Genome Biol.* **12**, R79 (2011).
51. Zisoulis, D. G. et al. Comprehensive discovery of endogenous Argonaute binding sites in *Caenorhabditis elegans*. *Nat. Struct. Mol. Biol.* **17**, 173–179 (2010).
52. Kim, D., Langmead, B. & Salzberg, S. L. HISAT: a fast spliced aligner with low memory requirements. *Nat. Methods* **12**, 357–360 (2015).
53. Anders, S., Pyl, P. T. & Huber, W. HTSeq—a Python framework to work with high-throughput sequencing data. *Bioinformatics* **31**, 166–169 (2015).
54. Meng, J. et al. A protocol for RNA methylation differential analysis with MeRIP-seq data and exomePeak R/Bioconductor package. *Methods* **69**, 274–281 (2014).
55. Weng, H. Y. et al. Inhibition of miR-17 and miR-20a by oridonin triggers apoptosis and reverses chemoresistance by derepressing BIM-S. *Cancer Res.* **74**, 4409–4419 (2014).
56. Eismann, T. et al. Peroxiredoxin-6 protects against mitochondrial dysfunction and liver injury during ischemia–reperfusion in mice. *Am. J. Physiol. Gastr. L.* **296**, 266–274 (2009).
57. Chen, B. et al. Dynamic imaging of genomic loci in living human cells by an optimized CRISPR/Cas system. *Cell* **155**, 1479–1491 (2013).
58. Slaymaker, I. M. et al. Rationally engineered Cas9 nucleases with improved specificity. *Science* **351**, 84–88 (2016).

nature research

Corresponding author(s): Jianjun Chen

☐ Initial submission ☐ Revised version ☒ Final submission

Life Sciences Reporting Summary

Nature Research wishes to improve the reproducibility of the work that we publish. This form is intended for publication with all accepted life science papers and provides structure for consistency and transparency in reporting. Every life science submission will use this form; some list items might not apply to an individual manuscript, but all fields must be completed for clarity.

For further information on the points included in this form, see Reporting Life Sciences Research. For further information on Nature Research policies, including our data availability policy, see Authors & Referees and the Editorial Policy Checklist.

Experimental design

1. Sample size

Describe how sample size was determined.

No sample size was pre-determined. Sample size and number of independent experiments are always clearly stated in the figure legend or in the Methods section.Three to more independent results were used to perform statistical analyses. If less, no statistics were performed from these samples. All raw data required for statistical tests are indicated in supplementary Table 3 (Statistics data source).

2. Data exclusions

Describe any data exclusions.

No data were excluded from analysis.

3. Replication

Describe whether the experimental findings were reliably reproduced.

Experiments in the article were reliably reproduced, replication were described in the figure legends.

4. Randomization

Describe how samples/organisms/participants were allocated into experimental groups.

No formal randomization techniques was used. No animals and/or human research participants were involved.

5. Blinding

Describe whether the investigators were blinded to group allocation during data collection and/or analysis.

Investigators were not blinded to group allocation during data collection and/or analysis.

Note: all studies involving animals and/or human research participants must disclose whether blinding and randomization were used.

6. Statistical parameters

For all figures and tables that use statistical methods, confirm that the following items are present in relevant figure legends (or in the Methods section if additional space is needed).

n/a	Confirmed
☐	☒ The exact sample size (*n*) for each experimental group/condition, given as a discrete number and unit of measurement (animals, litters, cultures, etc.)
☐	☒ A description of how samples were collected, noting whether measurements were taken from distinct samples or whether the same sample was measured repeatedly
☐	☒ A statement indicating how many times each experiment was replicated
☐	☒ The statistical test(s) used and whether they are one- or two-sided (note: only common tests should be described solely by name; more complex techniques should be described in the Methods section)
☐	☒ A description of any assumptions or corrections, such as an adjustment for multiple comparisons
☐	☒ The test results (e.g. *P* values) given as exact values whenever possible and with confidence intervals noted
☐	☒ A clear description of statistics including central tendency (e.g. median, mean) and variation (e.g. standard deviation, interquartile range)
☐	☒ Clearly defined error bars

See the web collection on statistics for biologists for further resources and guidance.

Software

Policy information about availability of computer code

7. Software

Describe the software used to analyze the data in this study.	Microsoft excel 2016 was used to calculate mean, standard deviation and P value. TotalLab 2.0 was used to quantify signal of gel shift assay. The custom Perl and R scripts used in this study are available on request to the corresponding authors.

For manuscripts utilizing custom algorithms or software that are central to the paper but not yet described in the published literature, software must be made available to editors and reviewers upon request. We strongly encourage code deposition in a community repository (e.g. GitHub). *Nature Methods* guidance for providing algorithms and software for publication provides further information on this topic.

Materials and reagents

Policy information about availability of materials

8. Materials availability

Indicate whether there are restrictions on availability of unique materials or if these materials are only available for distribution by a for-profit company.	No unique materials used in the study.

9. Antibodies

Describe the antibodies used and how they were validated for use in the system under study (i.e. assay and species).	Mouse anti-m6A antibody, Supplier: Synaptic Systems, Cat.: #202003, RRID: AB_2279214. Mouse anti-FLAG M2 antibody, Supplier: Sigma-Aldrich, Cat.: F3165, Clone: M2, Lot: SLBN8915V, RRID: AB_259529. Rabbit anti-IGF2BP1 antibody, Supplier: Cell Signaling Technology, Cat.: #8482, Clone: clone D33A2, Lot: 1. Rabbit anti-IGF2BP2 antibody, Supplier: Cell Signaling Technology, Cat.: #14672, Clone: clone D4R2F, Lot: 1. Rabbit anti-MYC antibody, Supplier: Cell Signaling Technology, Cat.: #13987, Clone: clone D3N8F, Lot: 1. Rabbit anti-HuR antibody, Supplier: Cell Signaling Technology, Cat.: #12582, Clone: clone D9W7E, Lot: 1. Rabbit anti-IGF2BP3 antibody, Supplier: Bethyl Laboratories, Cat.: A303-426A, RRID: AB_10951696. Rabbit anti-MATRIN3 antibody, Supplier: Bethyl Laboratories, Cat.: A300-591A-T, RRID: AB_495514. Rabbit anti-DCP1A antibody, Supplier: Bethyl Laboratories, Cat.: A303.590A-T, RRID: AB_11125540. Mouse anti-GAPDH antibody, Supplier: Santa Cruz Biotechnology, Cat.: sc-47724, Clone: 411, RRID: AB_627678. rabbit IgG, Supplier: Millipore, Cat.: #NI01, Lot: D00168753. HRP-conjugated anti-rabbit IgG secondary antibody, Supplier: Santa Cruz Biotechnology, Cat.: sc-2357, Lot: A1817. HRP-conjugated anti-mouse IgG secondary antibody, Supplier: Santa Cruz Biotechnology, Cat.: sc-2055, Lot: E1116. Alexa Fluor 488 anti-rabbit IgG, Supplier: Cell Signaling Technology, Cat.: #4412, Lot: 11. Alexa Fluor 594 anti-mouse IgG, Supplier: Cell Signaling Technology, Cat.: #8890, Lot: 2. Antibodies were validated by the use of negative control and/or positive control (such as knockdown or overexpression) for IGF2BP1, IGF2BP2, IGF2BP3, MYC, HuR and FLAG antibodies. Antibodies were used at 1:1000 dilution for western blot or at 1:200 for immuno staining, while 1 microgram or 10 microgram antibody was used for each co-IP/RIP or CLIP assay.

10. Eukaryotic cell lines

a. State the source of each eukaryotic cell line used.	All cell lines were purchased from the American Type Culture Collection (ATCC).
b. Describe the method of cell line authentication used.	Cell lines were not authenticated by ourselves.
c. Report whether the cell lines were tested for mycoplasma contamination.	All cell lines were tested to be mycoplasma negative.
d. If any of the cell lines used are listed in the database of commonly misidentified cell lines maintained by ICLAC, provide a scientific rationale for their use.	No cell lines used in this study were found in the database of commonly misidentified cell lines that is maintained by ICLAC and NCBI Biosample.

Animals and human research participants

Policy information about studies involving animals; when reporting animal research, follow the ARRIVE guidelines

11. Description of research animals

Provide details on animals and/or animal-derived materials used in the study.	No animals were used.

Policy information about studies involving human research participants

12. Description of human research participants

Describe the covariate-relevant population characteristics of the human research participants.	The study did not involve human research participants.